

Molecular origin of ^{31}P -NMR chemical shifts of phosphate groups with bivalent counter ions

Leo Christianell,^{†,‡} Karl-Jakob König,[†] Julian Holzinger,[†] Anne K. Schütz,[†] and Benjamin P. Fingerhut^{*,†,‡}

[†]*Department of Chemistry, Ludwig-Maximilians-Universität München, München, 81377, Germany*

[‡]*Center for NanoScience (CeNS), Schellingstr. 4, München, 80799, Germany*

E-mail: benjamin.fingerhut@cup.lmu.de

Abstract

The electrostatic interactions of phosphate groups and counter ions critically affect the structure, function and reactivity of DNA or RNA. We present a joint experimental-theoretical investigation of dimethyl phosphate (DMP^-) in aqueous solution, an established model system of the sugar-phosphate backbone. Utilizing ^{31}P -NMR spectroscopy as probe of phosphate-ion association, variations of Mg^{2+} and Ca^{2+} content exhibit a systematic shielding of the ^{31}P chemical shift ($\delta_{iso}(^{31}\text{P})$) with moderate temperature dependence. Enhanced sampling molecular dynamics (MD) and ab initio (GIAO-DF-LMP2) level of theory are used to reveal the microscopic mechanism. Simulations are performed for a configurational ensemble of DMP^- -ion geometries and their first solvation shells, demonstrating (i) the spatial convergence of changes of the nuclear shielding constant $\sigma_{iso}(^{31}\text{P})$, (ii) the intramolecular geometric origin of short-timescale $\sigma_{iso}(^{31}\text{P})$ fluctuations and (iii) an average shift of $\sigma_{iso}(^{31}\text{P})$ of about 3-5 ppm upon contact ion pair formation with Mg^{2+} or Ca^{2+} ions. A quantitative analysis of $\delta_{iso}(^{31}\text{P})$ for varying ion content and temperature allows us to extract the temperature-dependent fraction of the contact ion pair species, indicating that solvent separated or free ion pairs are the energetically preferred species. The results impose boundary conditions for improvements of phosphate ion force fields and establish the interactions underlying the changes of $\delta_{iso}(^{31}\text{P})$.

Introduction

The polyanionic structures of DNA and RNA are stabilized via electrostatic interactions with counter ions.^{1,2} In this context, bivalent counter ions like Mg^{2+} are particularly important for neutralizing the negative charge density of the phosphate (PO_2) groups, thereby facilitating the folding of complex RNA structures.^{3,4} Moreover, metal ions are directly involved in the catalytic function of RNA.⁵⁻⁷ Charge neutralization of DNA or RNA occurs on a length scale of about 2 nm from surface.^{8,9} It gives rise to an ion atmosphere around the polyanion that is made up from the distinct species of contact ion pairs (CIP) and solvent shared

ion pairs (SSIP). Both species form specific hydrogen bond interactions, whereas weakly bound ions interact via *unspecific* (Coulombic) interactions. In CIPs the cation is partially dehydrated and interacts directly with one of the non-bridging oxygens of the PO_2 group (inner-sphere coordination), while in SSIPs the cation retains its full solvation shell (outer-sphere coordination). In RNA about 10% of bivalent ions are estimated to be site specifically bound.¹⁰

Ion counting experiments¹¹⁻¹⁴ provide quantitative access to the total number of ions interacting with the polymer, demonstrating that Mg^{2+} binds stronger to RNA than DNA,^{15,16} without the ability to distinguish specific interacting species, i.e., CIP and SSIP on the molecular level. Recently, infrared (IR) and non-linear two-dimensional IR (2D-IR) spectroscopy together with in-depth theoretical analysis suggested the presence of CIP species for double-stranded RNA¹⁷ and transfer RNA (tRNA),¹⁸ and a molecular electrostatic scenario at the surface of the biomolecules not reproduced by Poisson-Boltzmann theory. CIP of Mg^{2+} with PO_2 groups have the ability to strongly modulate the local electrostatic potential, thereby facilitating the close approach of PO_2 groups in kink and bulge regions of folded RNA. The specific detection of CIP in the biomolecules relied on a characteristic blue-shift of the asymmetric PO_2 stretching vibration, that showed a number of CIP consistent with fluorescence titration experiments. Analogous observations of a blue-shifted asymmetric PO_2 stretching vibration for ionic (Na^+ , Mg^{2+} , Ca^{2+}) solutions of DMP^- ,¹⁹⁻²¹ a well established model system of the sugar-phosphate backbone of DNA and RNA,²²⁻²⁵ allowed for rigorous simulation access to the origin of the blue shift of the vibration. Microscopically, the close proximity of the Mg^{2+} ion and the non-bridging oxygen atom of the PO_2 group ($\text{P-O}^- - \text{Mg}^{2+}$ distance $\approx 2.1 \text{ \AA}$) leads to an asymmetric distortion of the PO_2 bonding potential due to exchange repulsion interactions at short inter-molecular distances. Estimates utilizing the amplitudes of IR and 2D-IR spectroscopy suggested the formation of CIP species in a 10-30 % range for 10 equivalents (eq.) excess ion concentration relative to the 0.2 M concentration of DMP^- . Kutus and coworkers recently derived ion pairing equilibria of Na^+ , Mg^{2+} and Ca^{2+} with

DMP⁻ from dielectric relaxation spectroscopy.²⁶ Respective association constants relied on estimates of dipole moments of dipole-bound complexes from density functional theory and allowed to derive ion pair lifetimes of 330 ps for Na⁺DMP⁻ and 700 ps for Ca²⁺DMP⁻, while Mg²⁺ DMP⁻ lifetime estimates were consistent with > 1 μ s estimates.

Utilizing the spin 1/2 ³¹P nucleus of the phosphate group, NMR spectroscopy has long been used for detecting metal ions, in particular Mg²⁺ interactions with DNA or RNA²⁷⁻³⁰ and to rank Mg²⁺ binding sites in the polyphosphate chain.²⁹ Haake and coworkers³¹ suggested a two-component model to extract association constants, by utilizing the ³¹P chemical shift with increasing ion concentration, the latter being tentatively assigned to ion pairing. A similar model yielded association constants of DMP⁻ and ions that are largely consistent between ³¹P-NMR and dielectric relaxation spectroscopy.²⁶ Besides these quantitative approaches to ion pairing, NMR experiments characterized numerous ion binding sites.³²⁻³⁴ Nevertheless, the quantitative interpretation of observed ³¹P chemical shifts is still complicated by a limited microscopic understanding of their origin, in particular the dependence of chemical shifts on sugar-phosphate conformation and sensitivity to ionic interactions. Moving beyond structure to chemical reactivity, in particular phosphoryl cleavage and transfer reactions, a deeper understanding of the origin of ³¹P chemical shifts could elucidate biocatalytic mechanisms.^{35,36}

Concerning the association of PO₂ groups with bivalent cations Mg²⁺ and Ca²⁺, substantial uncertainty remains regarding their tendency to form CIP structures. Ion association constants from dielectric relaxation spectroscopy suggest largely similar properties for Mg²⁺ and Ca²⁺.²⁶ MD simulations with a fixed-charge force field, utilizing ion parameters by Li *et al.*,³⁷ suggest a stronger tendency for Mg²⁺ than Ca²⁺ to compress and assemble DNA strands into compact structures.³⁸ A recent re-parametrization of the 12-6-4 non-bonding model by the Merz group,³⁹ based on ion binding free energy energies for dihydrogen-phosphate (H₂PO₄⁻), suggests a stronger binding of Mg²⁺ to phosphates, compared to Ca²⁺. For both bivalent ions, CIP are substantially more stable than SSIP. Compared to DMP⁻, the asym-

metric PO_2 stretching vibration of H_2PO_4^- has a substantially more complex vibrational structure,^{40,41} where water molecules in the first solvation shell donate hydrogen bonds to the PO_2 moiety and accept hydrogen bonds from the O-H groups of H_2PO_4^- , a scenario not realized in DMP^- and to which extent the hydrogen bond donor functionality³⁹ of H_2PO_4^- affects the relative stability of CIP and SSIP is an open question.

A recent re-parametrization of DMP^- with the polarizable amoeba model²⁴ provided reasonable values of ion binding free energy energies of DMP^- with Mg^{2+} and Ca^{2+} , respectively. Nevertheless, the refined force field tends to underestimate the population of CIP, compared to estimates derived from 2D-IR experiments, indicating an over-stabilization of the SSIP species. To the contrary, theoretical work utilizing the reference interaction site model suggests that Ca^{2+} ions have a preference for CIP formation over Mg^{2+} ions.⁴² Force fields used in MD simulations of ion association around DNA and RNA thus still have limited predictive accuracy in describing the interactions of phosphate groups with doubly charged ions. Further experimental benchmark data on the relative stability of CIP and SSIP species and the behaviour concerning the differences of bivalent ions are highly desirable.

In this work we present the temperature dependence of ^{31}P chemical shifts in DMP^- for a wide range of Mg^{2+} concentrations and compare to measurements with other ions (Ca^{2+} , Zn^{2+} , Cd^{2+} , Na^+ and $[\text{Co}(\text{NH}_3)_6]^{3+}$). The observations are analyzed in ab initio simulations investigating the convergence of the quantum mechanical interaction region and basis set dependence. The origin of the observed chemical shift is microscopically assigned to the formation of the CIP species, which is distinct from the effect of geometric distortions of DMP^- . Utilizing a two-component model, we further establish the relative population $X[\text{CIP}]$ of CIP with Mg^{2+} and Ca^{2+} ions, which in turn imposes boundary conditions on the potential of mean force of ion binding.

Materials and Methods

NMR spectroscopy

Reagent preparation

Chemicals were bought from Grüssing (Filsum, Germany), Sigma-Aldrich (Darmstadt, Germany) and Santa Cruz Biotechnology (Dallas, USA) and used as received. D₂O (99.9 % D) was purchased from Deutero (Kastellaun, Germany). Hexaamminecobalt(III) chloride was synthesized according to a modified literature synthesis⁴³ by oxidation of an aqueous solution of Cobalt(II) chloride with hydrogen peroxide in presence of ammonium chloride, activated charcoal and ammonia at 0 °C. A pure product could be obtained by precipitation with hydrochloric acid, followed by filtration with hot hydrochloric acid and recrystallization in ethanol.

NMR experiments

All NMR spectra were acquired on a Bruker Avance III HD 400 MHz spectrometer (9.4 T), using a broadband BBO 400S1 probe. The measurements were set up, performed and evaluated using Bruker TopSpin 3.5. Relaxation data were analyzed with Dynamics Center 2.1.8. The temperature was regulated using the spectrometer's internal temperature control, after calibration with methanol and ethylene glycol.^{44,45} ¹H spectra were first recorded without water suppression to obtain the shift of the maximum water peak height. This value was used as the offset for a second ¹H spectrum to ensure the maximum water signal reduction via the WATERGATE pulse sequence. The ¹H pulse length was optimized after every titration step. ¹³C Spectra were obtained with a fixed 30° pulse. ³¹P Spectra were acquired both with and without ¹H garp decoupling. *T*₁ and *T*₂ relaxation times were measured for ³¹P at 25 °C in all ion titrations. The inversion recovery method was used to determine *T*₁ relaxation times. The Carr-Purcell-Meiboom-Gill (CPMG) pulse sequence was used to determine *T*₂ relaxation times using (20 ms π 20 ms) spin echo blocks. A monoexponential

decay function was fitted to the signal intensities. Chemical shifts were referenced against 3-(trimethylsilyl)-1-propanesulfonic acid sodium salt (DSS) for the initial spectra. Linewidths were automatically determined as full width at half height (FWHH) using the peakw command from TopSpin. For signals where the automatic FWHH determination failed due to broadness or overlap, the linewidths were determined manually.

Titration experiments

Samples of sodium dimethyl phosphate (NaDMP) for titrations were prepared by adding 450 μ L of a 9:1 $\text{H}_2\text{O}:\text{D}_2\text{O}$ mixture to NaDMP powder (0.09 mmol, 0.01332 g, 0.2 M) in a 5 mm NMR tube with an additional 1 μ L of 1 mM DSS solution. Stocks solutions with dissolved metal ion salts were titrated to achieve the required concentrations. Where applicable, the samples were measured at each reported temperature before adding new stock solution. The respective molar ratios $n(\text{ion})/n(\text{DMP}^-)$ were expressed as equivalents (eq.) of metal ions to DMP^- . Series from 0.1 eq up to 25 eq were measured, depending on the effect of the metal ions on the NMR spectra. Stocks solutions of the used ions and respective salts are summarized in Table 1.

Table 1: Summary of the metal ion stock solutions used in the NMR experiments.

Metal ion	Salt	Stock concentration / M
Mg^{2+}	MgCl_2	4.07
Ca^{2+}	CaCl_2	6.00
Cd^{2+}	CdI_2	0.50
$[\text{Co}(\text{NH}_3)_6]^{3+}$	$[\text{Co}(\text{NH}_3)_6]\text{Cl}_3$	0.25
Zn^{2+}	ZnCl_2	3.57
Na^+	NaCl	4.94

Simulations

Molecular Dynamics Simulations

Atomistic MD Simulations were performed with the MPI implementation of the Amber18 and Amber24 software packages⁴⁶ and employed the parmbsc1 DNA force field parameters⁴⁷ and partial charges of the phosphate group for DMP⁻ together with the TIP4P-FB water model⁴⁸ and corresponding 12-6-4 Lennard-Jones parameters for mono and divalent ions.^{37,49,50} Systems were created with the LEaP software included in AmberTools24.⁵¹ Analysis and visualization of the trajectories were carried out with pytraj as Python package binding to the cpptraj program⁵² and VMD.⁵³

Solvatization of the systems was realized in a truncated octahedron box with a minimum buffer size of 20 Å. Sodium cations or chloride anions were added for charge neutralization. A cut-off criterion of 9 Å was imposed on the non-bonded interactions and long-range Coulomb interactions were treated with the particle mesh Ewald summation method.^{54,55} A time step of 2 fs was used for the integration of motions while all bonds including hydrogen and all water molecules were constrained with the SHAKE⁵⁶ and SETTLE⁵⁷ algorithms, respectively. All systems were optimized in a three-step approach by first applying harmonic positional constraints of 100 kcal mol⁻¹ Å⁻² on the solute atoms to allow relaxation of the solvent (10000 steps) followed by a second optimization with reduced harmonic restraints of 10 kcal mol⁻¹ Å⁻² (10000 steps) and a third constraint free optimization (10000 steps). After half of the respective optimization steps, the algorithm was switched from the steepest descent to the conjugated gradient method. The systems were heated over 0.2 ns to the target temperature of 298 K using the Langevin thermostat⁵⁸ employing a collision frequency of 1 ps⁻¹ which was followed by 0.6 ns of pressure equilibration to 1 bar with the Berendsen barostat⁵⁹ using a pressure coupling constant of 1 ps. During this equilibration period, harmonic positional constraints of 100 kcal mol⁻¹ Å⁻² were applied to the solute atoms which were gradually removed over the following 1.2 ns resulting in a final 1.2 ns unrestrained

equilibration in the NpT ensemble. The unbiased DMP^- , $\text{DMP}^- - \text{Mg}^{2+}$ and $\text{DMP}^- - \text{Ca}^{2+}$ systems were sampled for 10 ns.

Umbrella sampling was performed with the non-bridging DMP^- -O1 - Mg^{2+} distance (force field atom type O1P, see Fig. 1,a for labeling) as reaction coordinate along which the potential of mean force (PMF) was evaluated from 2.00 Å to 6.00 Å ($\Delta d = 0.1 \text{ \AA}$). A distance based restraint of $300 \text{ kcal mol}^{-1} \text{ \AA}^{-2}$ was imposed on a virtual O1 - Mg^{2+} bond. Each distance was initially re-equilibrated for at least 0.1 ns, starting from the nearest available distance sampling point with a subsequent sampling period of 10 ns. To avoid unwanted interactions between Mg^{2+} and the second non-bridging oxygen atom O2 of DMP^- (force field atom type O2P), a repulsive harmonic potential between DMP^- -O2 - Mg^{2+} with a force constant of $30 \text{ kcal mol}^{-1} \text{ \AA}^{-2}$ was applied if the respective distance fell below 3.4 Å. Distance information was saved every 0.1 ps. The unbiasing of the umbrella sampling runs was performed with the vFEP^{60,61} routine with Jacobian corrections to obtain the free energy landscape.

Ab initio simulations of NMR shielding constants (see below, Fig. 3,a) were performed with a sampling of linear P-O1-Mg²⁺ configurations. Starting structures were taken from the umbrella sampling runs and $600 \text{ kcal mol}^{-1} \text{ \AA}^{-2}$ angular and distance based harmonic restraints were subsequently applied to the P-O1-Mg²⁺ atoms. The systems were re-equilibrated for 0.4 ns, followed by 10 ns production sampling runs, coordinates were saved every 20 ps.

Ab Initio Simulations

Nuclear shielding constants $\sigma_{iso}^{(31\text{P})}$ were calculated on the GIAO-DF-LMP2 ab initio level of theory^{62,63} implemented in Molpro 2024.1.^{64,65} GIAO-MP2 simulations generally provide accurate chemical shifts (comparable or superior to DFT) over a broad range ($\sim 600 \text{ ppm}$) of phosphorus shielding constants,⁶⁶ particularly when used with large basis sets and the GIAO-DF-LMP2 approximation retains very high accuracy.⁶³ In benchmark simulations we tested the quality of the basis set for $\sigma_{iso}^{(31\text{P})}$ and investigated the influence of the size of hydration

shell. Benchmark simulations were performed on a randomly chosen configuration of a DMP^- - Mg^{2+} CIP and free DMP^- from MD simulations. Correlation-consistent polarized Dunning basis sets with core correlation (cc-pCVXZ, X=D,T,Q,5) were used for heavy atoms, while for hydrogen atoms cc-pVXZ (X=D,T,Q,5) were used. For density fitting⁶⁷ the corresponding basis sets without core correlation were applied. Benchmarks have shown an insignificant contribution of the density fitting basis set on the nuclear shielding constants. As simulations on the GIAO-DF-LMP2 level of theory are computationally expensive, in particular for system sizes with large hydration shell (see below), we additionally benchmarked mixed basis sets where hydrogen atoms were treated with double zeta accuracy (cc-pVDZ).

The influence of an explicit solvent shell on $\sigma_{iso}(^{31}\text{P})$ of DMP^- was benchmarked for DMP^- - Mg^{2+} CIP, DMP^- - Ca^{2+} CIP and free DMP^- . The hydration shells were constructed with a distance based cut-off criterion from the surface of the solute molecules (DMP^- - Mg^{2+} CIP, DMP^- - Ca^{2+} CIP or DMP^-). Nuclear shielding constants were averaged over 100 configurations taken from MD simulations with a relative spacing of 0.1 ns to assure uncorrelated configurations. Due to convergence issues four DMP^- - Ca^{2+} configurations were discarded. To quantify the influence of the hydration shell on $\sigma_{iso}(^{31}\text{P})$, respective vacuum systems of DMP^- - Mg^{2+} CIP, DMP^- - Ca^{2+} CIP and DMP^- were constructed by removing the solvent molecules.

Atomic partial charges were evaluated using the Mulliken charges routine in Molpro. Partial charges were averaged over the same configurations as used in the chemical shielding simulations. The partial charges of DMP^- - Mg^{2+} and DMP^- - Ca^{2+} CIP were averaged over 100 MD snapshots with a 4.5 Å hydration shell, five Ca^{2+} configurations were discarded for convergence issues.

For a mapping of the ^{31}P chemical shift on geometric parameters, P-O distances of DMP^- were scanned in a range 1.35 Å to 1.60 Å for O1/O2-P non-bridging oxygen atoms ($\Delta d=0.01$ Å) and 1.40 Å to 1.80 Å for O3/O5-P bridging oxygen atoms ($\Delta d=0.04$ Å) and $\sigma_{iso}(^{31}\text{P})$ were evaluated for every geometry (cc-pCVTZ). Test simulations showed that the

influence of the O-P-O angle on $\sigma_{iso}(^{31}\text{P})$ is minor which was thus neglected. Chemical shift mapping was performed by assigning the instantaneous DMP^- configuration to the nearest grid point on the 4-D nuclear shielding map $\sigma_{iso}^{pred}(^{31}\text{P})(r_{O1-P}, r_{O2-P}, r_{O3-P}, r_{O5-P})$ (82000 points).

Table 2: Average change of atomic partial charges Δq upon CIP formation in DMP^- - Mg^{2+} and DMP^- - Ca^{2+} with a 4.5 Å hydration shell on HF and GIAO-DF-LMP2 level of theory.

Atom	Δq (HF) / e^-		Δq (LMP2) / e^-	
	Mg^{2+}	Ca^{2+}	Mg^{2+}	Ca^{2+}
P	-0.051	0.013	-0.014	-0.177
O1	0.154	0.056	0.138	0.110
O2	-0.006	-0.011	-0.004	0.031
I^{2+}	-0.045	-0.035	-0.126	-0.128

Results

Concentration and temperature dependence of ^{31}P chemical shifts

A central question concerns the sensitivity of ^{31}P NMR observable to detect in a species selective manner CIP or SSIP of the PO_2 group with bivalent ions. Observed changes of ^{31}P chemical shifts $\delta(^{31}\text{P})$ arise due to the high sensitivity of the 1/2 spin nucleus to the local molecular environment that is affected by hydration species, the DMP^- conformation and electronic density changes from specific interactions of ions with the PO_2 group (exemplary structures of DMP^- - Mg^{2+} CIP and SSIP are depicted in Figure 1,b-c). We measured the isotropic chemical shift of the ^{31}P nucleus ($\delta_{iso}(^{31}\text{P})$) for 0.2 M NaDMP dissolved in water as a function of counter ion concentration and temperature. Under such low concentration condition of Na^+ DMP^- association is minor²⁶ and the effect on $\delta_{iso}(^{31}\text{P})$ is negligible.

Figure 1,e presents the $\delta_{iso}(^{31}\text{P})$ for varying Mg^{2+} concentration in the range 0 to 25 eq. at 298 K without ^1H decoupling. At low Mg^{2+} content (≤ 2 eq.), the septet is caused by the $^3\text{J}_{PH}$ coupling of the ^{31}P spin to the six magnetic equivalent ^1H . $\delta_{iso}(^{31}\text{P})$ peak

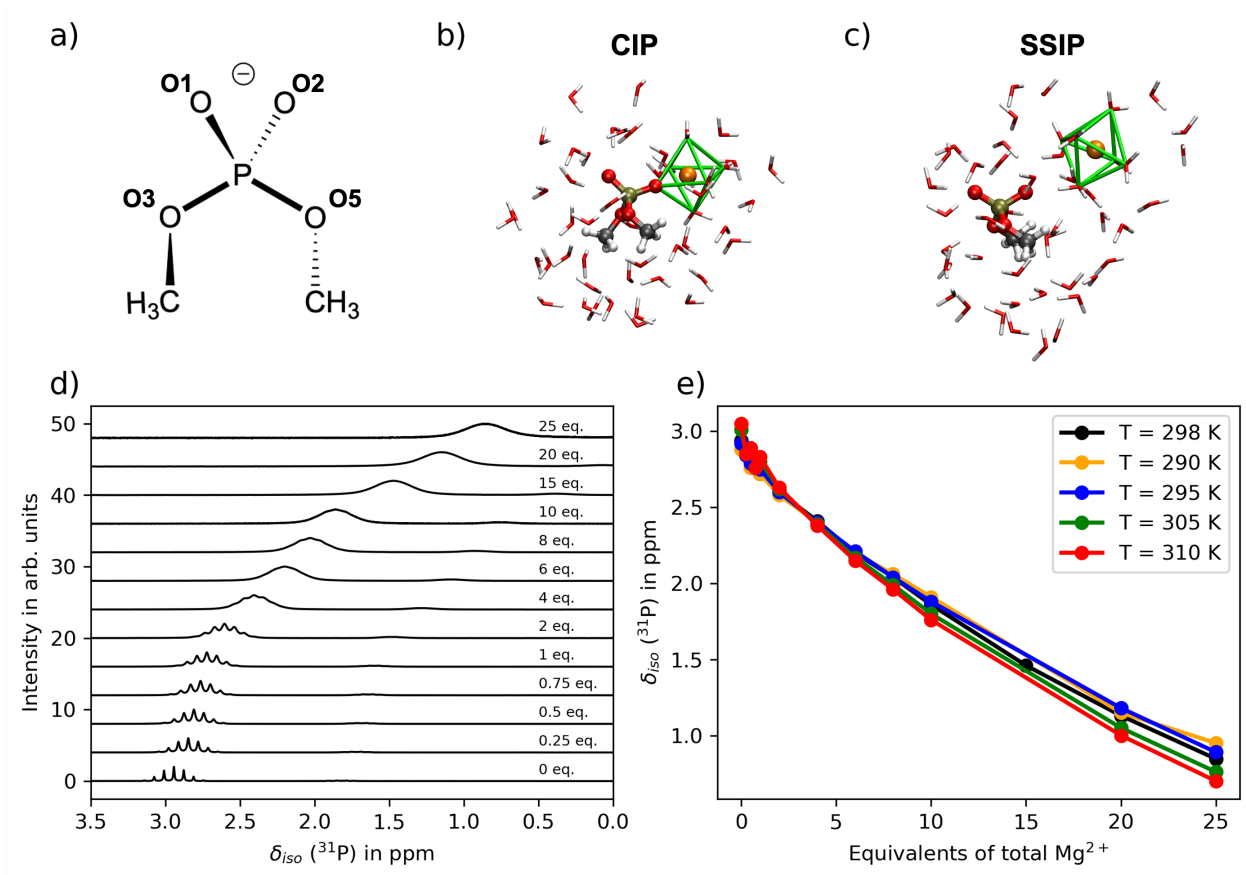


Figure 1: Experimental $\delta_{iso}^{(31)P}$ of DMP⁻ upon titration with Mg²⁺. (a) Atomic labeling of DMP⁻. (b,c) Snapshots of DMP⁻ - Mg²⁺ CIP and SSIP from MD simulations. The octahedral solvation shell of Mg²⁺ is highlighted in green, i.e., MgO1(H₂O)₅ and Mg(H₂O)₆. (d) Experimental ³¹P-NMR spectra measured in the range 0 to 25 eq. of Mg²⁺ at 298 K. (e) Peak positions of $\delta_{iso}^{(31)P}$ in a temperature range from 290 K to 310 K and 0 to 25 eq. of Mg²⁺.

positions derived from ^1H -decoupled and ^1H non-decoupled NMR spectra (see Materials and Methods Section) essentially coincide. For Mg^{2+} content > 4 eq., a broadened unstructured ^{31}P resonance is observed, which is increasingly shielded with a further increase of Mg^{2+} . Changes in the linewidth of the ^{31}P -NMR spectra are associated either with changes of the transverse relaxation rate R_2 or with chemical exchange (e.g. Mg^{2+} -bound and free DMP^-) or a combination of both (cf. Table 3).

Figure 1,d depicts the peak position of $\delta_{iso}(^{31}\text{P})$ for varying Mg^{2+} concentration and temperature in a range 290–310 K. The overall range of $\delta_{iso}(^{31}\text{P})$ covers a shift of about 2.5 ppm that is moderately increased (≈ 0.4 ppm) with increasing temperature and $\delta_{iso}(^{31}\text{P})$ does not approach saturation, even for 25 eq. of Mg^{2+} .

Table 3 summarizes the experimental results for ions Mg^{2+} , Ca^{2+} , Na^+ , Zn^{2+} , Cd^{2+} , $[\text{Co}(\text{NH}_3)_6]^{3+}$. Major changes of $\delta_{iso}(^{31}\text{P})$ are observed for Mg^{2+} , Ca^{2+} and $[\text{Zn}^{2+}]$ while for Cd^{2+} , $[\text{Co}(\text{NH}_3)_6]^{3+}$ and Na^+ changes of $\delta_{iso}(^{31}\text{P})$ are smaller by about an order of magnitude. Similar trends are observed for the longitudinal relaxation rate R_1 and transverse relaxation rate R_2 where Mg^{2+} and Zn^{2+} show changes that are substantially larger than that for Cd^{2+} , $[\text{Co}(\text{NH}_3)_6]^{3+}$ and Na^+ , correspondingly reflected in the changes of the linewidth.

Table 3: ^{31}P -NMR observables for 0 eq. (reference) and 4 eq. of the respective ion at 298 K. R_1 denotes the longitudinal relaxation rate and R_2 the transverse relaxation rate, $\Delta\delta_{iso}$ is the change in chemical shift with respect to 0 eq. of the ions. Zn^{2+} is indicated for 0.1 eq. as data analysis at higher concentrations was prevented by strong line broadening. The observed R_2 relaxation rate is the sum of intrinsic relaxation rate plus a possible exchange contribution.

Metal ion	δ_{iso} / ppm	R_1 / Hz	R_2 / Hz	linewidth / Hz	$\Delta\delta_{iso}$ / ppm
0 eq. (ref.)	2.94	0.09	0.28	0.40	–
Mg^{2+}	2.41	0.19	27.78	14.85	-0.53
Ca^{2+}	2.57	0.11	0.71	1.55	-0.37
Cd^{2+}	2.98	0.09	0.57	2.64	0.04
$[\text{Co}(\text{NH}_3)_6]^{3+}$	2.90	0.09	0.96	1.98	-0.04
Zn^{2+}	2.92	0.33	69.93	25.54	-0.02
Na^+	3.01	0.09	0.33	2.98	0.07

¹Note that difficulties from strong linebroadening for Zn^{2+} limited the analysis to <0.1 eq

Solvent shell and geometric dependence of the ^{31}P chemical shift

Spatial interaction range

To obtain a microscopic understanding of the observed shift of $\delta_{iso}(^{31}\text{P})$ with increasing Mg^{2+} content, we investigated in ab initio simulations the convergence of the isotropic ^{31}P shielding constant ($\sigma_{iso}(^{31}\text{P})$) for a quantum mechanical interaction range of increasing size. Experimentally measured $\delta_{iso}(^{31}\text{P})$ are related to the microscopic quantity $\sigma_{iso}(^{31}\text{P})$ as⁶⁶

$$\delta_{iso}(^{31}\text{P}) \approx \sigma_{iso}^{Ref}(^{31}\text{P}) - \sigma_{iso}(^{31}\text{P}) \quad (1)$$

where in experiments phosphoric acid is used as reference. The hydration environment of a $\text{DMP}^- - \text{Mg}^{2+}$ CIP was sampled from a classical molecular dynamics trajectory, taking into account $\text{DMP}^- - \text{Mg}^{2+} \times \text{N}(\text{H}_2\text{O})$ clusters of increasing size, with the largest clusters containing 60 water molecules (5.5 Å water shell, see Material and Methods Section), required to form about three hydration shells around the CIP. The results of the $\text{DMP}^- - \text{Mg}^{2+}$ CIP are compared to $\text{DMP}^- \times \text{N}(\text{H}_2\text{O})$ clusters, describing the hydration environment of free DMP^- in aqueous solution.

Figure 2,a depicts $\sigma_{iso}(^{31}\text{P})$ for an increasing solvation shell around the $\text{DMP}^- - \text{Mg}^{2+}$ CIP. Initially, the addition of a few discrete H_2O molecules decreases $\sigma_{iso}(^{31}\text{P})$ by about 2–3 ppm (2–3 Å solvation shell). Due to H_2O belonging to the second and third solvation shell, σ_{iso} is moderately increased by about 1 ppm, leading to convergence of $\sigma_{iso}(^{31}\text{P})$ on a spatial 4.5–5 Å range, where a complete second and third solvation shell, containing about 50-60 H_2O molecules, are formed around the CIP. In comparison, the hydration environment around free DMP^- (black dots in Fig. 2,a) first induces a shielding by about 2 ppm from the addition of discrete water molecules that converges on a very similar spatial range of 4.5–5 Å, i.e., for a hydration environment consisting of three solvation shells. The results demonstrate, that $\sigma_{iso}(^{31}\text{P})$ is particularly sensitive to details of the local environment: Changes of the charge density of the PO_2 group are induced by the first, second and third solvation shell,

successively defining its polarization, which is reflected in 2–3 ppm changes of $\sigma_{iso}(^{31}\text{P})$. The ^{31}P nucleus thus acts as local probe for environmental changes imprinted on the charge density of the PO_2 group, limited to a $< 5 \text{ \AA}$ range.

Additionally, we explored the effect of size of the basis set on simulated $\sigma_{iso}(^{31}\text{P})$ in a $\text{DMP}^- - \text{Mg}^{2+}$ CIP with a 3.0 and 4.5 \AA water shell, respectively (Fig. 2,b). While there is a substantial influence of basis set size (up to 40 ppm), when going from double zeta to triple zeta quality, changes are more moderate when comparing the results of triple and quadruple zeta (triangles in Fig. 2,a). Comparison of quintuple and quadruple basis set for the $\text{DMP}^- - \text{Mg}^{2+}$ CIPs with a 3.0 \AA hydration shell demonstrates that the quadruple zeta basis set yields essentially converged results.

A mixed-valence basis set has the potential to reduce the numerical effort, especially for $\text{DMP}^- - \text{Mg}^{2+}$ CIPs with large (4.5 \AA) hydration shell, where triple and quadruple zeta basis sets correspond to ≈ 4300 and 7500 basis functions, respectively. We find that reducing the basis to pVDZ quality for hydrogen atoms has a minor effect on $\sigma_{iso}(^{31}\text{P})$ (compare triangles and dots in Fig. 2,b). As the total basis set size can be substantially reduced (e.g. 4900 vs. 3600 basis functions for pCVQZ and pCVQZ/pVDZ, respectively), ^{31}P chemical shifts can be simulated rather efficiently with a mixed basis. Absolute errors by a mixed pCVQZ/pVDZ basis treatment are on the order of 0.5 ppm, comparable to the error of the GIAO-DF-LMP2 ab initio method.⁶³

Dependence of $\sigma_{iso}(^{31}\text{P})$ on intra-molecular degrees of freedom and $\text{DMP}^- - \text{Mg}^{2+}$ separation

The above results demonstrate that reasonably efficient but accurate simulations of $\sigma_{iso}(^{31}\text{P})$ can be achieved with a 4.5 \AA solvation shell around CIP and using a mixed pCVTZ/pCVDZ basis for heavy elements carbon and phosphorous, and hydrogen atoms, respectively. To investigate differences of $\sigma_{iso}(^{31}\text{P})$ for CIP, SSIP and fully solvated DMP^- hydration geometries, we performed large scale sampling of hydration geometries along a reaction coordinate

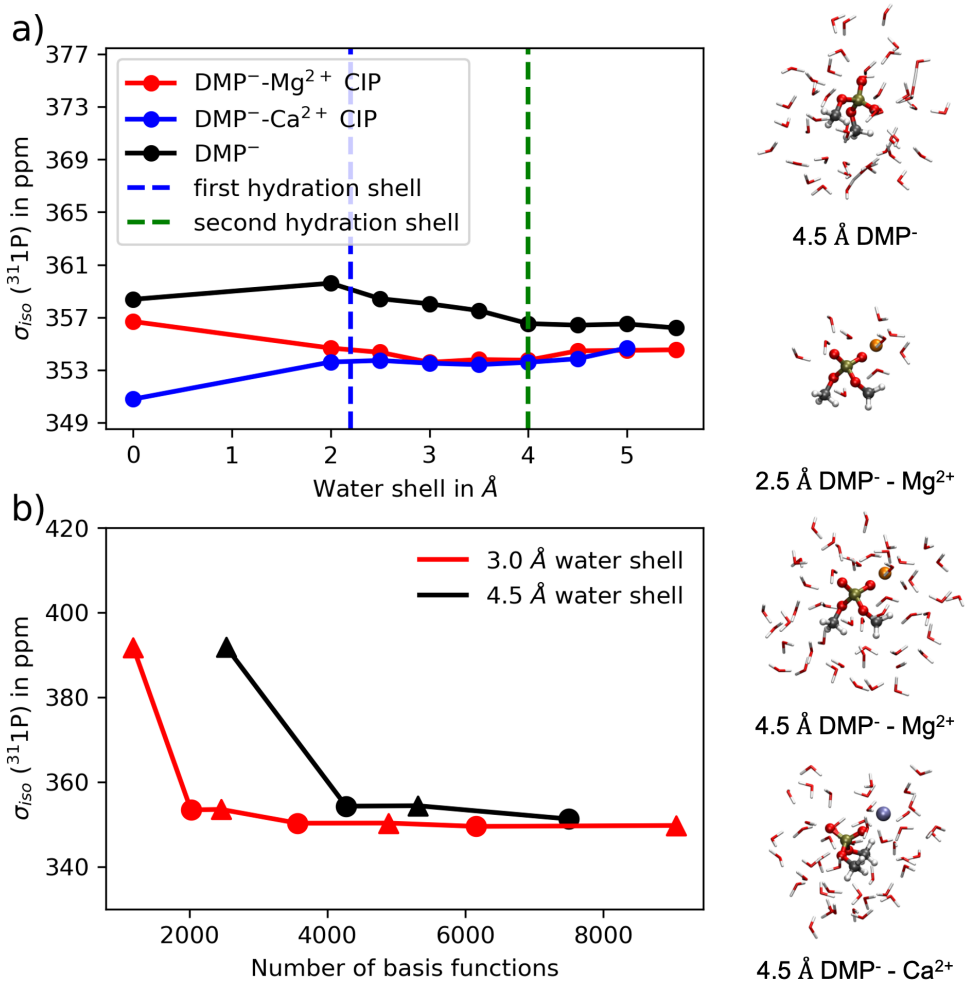


Figure 2: Benchmark of hydration shell and basis set. (a) Variation of $\sigma_{iso}(^{31}P)$ in a randomly chosen DMP⁻ - Mg²⁺ CIP configuration (red), DMP⁻ - Ca²⁺ CIP configuration (blue) and free DMP⁻ (black) with increasing size of the hydration shell (basis: pCVTZ). Dashed vertical lines indicate the first and second hydration shell, consisting of 6 and 36 H₂O (DMP⁻ - Mg²⁺ CIP); the largest cluster with 5 Å water shell considers 60 H₂O. (b) Benchmark of $\sigma_{iso}(^{31}P)$ in the DMP⁻ - Mg²⁺ CIP for varying basis size pCVXZ (X=D, T, Q, 5) basis set with a 3.0 Å (red) and 4.5 Å water shell (black). Triangles indicate a uniform pCVXZ basis set for all atom types and circles indicate a mixed basis set with pVDZ employed for hydrogen atoms. The right panel shows DMP⁻ \times N H₂O and DMP⁻ - I²⁺ CIP \times N H₂O (I = Mg, Ca) cluster snapshots for hydration shells of varying size.

obtained by umbrella sampling MD simulations (see Simulation Details). For each DMP^- - Mg^{2+} separation in the range [2-6] Å, we sampled 100 independent solvent configurations (0.1 ns separation, 4.5 Å solvation shell, up to 60 H_2O molecules) and evaluated $\sigma_{iso}^{(31\text{P})}$ along the reaction coordinate (2100 simulations total).

Figure 3,a shows the mean (dots) and width (bars, standard deviation) of the $\sigma_{iso}^{(31\text{P})}$ distributions as a function of DMP^- - Mg^{2+} separation. For all separations, the width of distributions covers about 10-12 ppm, much broader than the ≈ 0.2 ppm width observed in the NMR-experiments for Mg^{2+} contents < 2 eq (cf. Fig. 1). The mean of the distributions shows a systematic shift from 356.3 ppm (DMP^- - Mg^{2+} separation: 2 Å), to 351.2 ppm (DMP^- - Mg^{2+} separation: 6 Å). We have verified via the moving mean, that the center of respective $\sigma_{iso}^{(31\text{P})}$ distributions is converged within 0.2 ppm (cf. Fig. 3,b).

Configurational sampling of the reaction coordinate of DMP^- - Mg^{2+} separation employs an ensemble of instantaneous geometries with varying DMP^- bond lengths. Microscopic understanding of the distributional widths was then obtained from the dependence of $\sigma_{iso}^{(31\text{P})}$ on the intra-molecular degrees of freedom, the length of non-bridging O1/O2-P bonds and bridging O3/O5-P bonds, as well as O1-P-O2 and O3-P-O5 bond angles and C-O3-O5-C dihedral angles (cf. inlays in Fig. 3,b-d). We find that $\sigma_{iso}^{(31\text{P})}$ shows particular sensitivity to the O1/O2-P bond lengths and to a lower extend to the O3/O5-P bond lengths ($>$ tens of ppm, see below), while the sensitivity on bond angles and the C-O3-O5-C dihedral angle is less pronounced (≈ 4 ppm in the relevant angle distribution). Figure 3,c-d present the dependence of $\sigma_{iso}^{(31\text{P})}$ on respective bond lengths O1/O2-P and O3/O5-P. The 2D-surfaces show a strong dependence on the particular DMP^- geometry with a monotonous decrease of $\sigma_{iso}^{(31\text{P})}$ upon elongation of the bond lengths, spanning a > 50 ppm range for O1/O2-P distances and > 30 ppm range for O3/O5-P distances (DMP^- equilibrium geometry: O1/O2-P bond length = 1.48 Å, O3/O5-P bond length = 1.60 Å). Comparison with the distribution of sampled bond lengths (blue and green points in Fig. 3,c-d) shows that substantial width of the 2D-surfaces is explored due to the flexibility of DMP^- in MD simulations. As P=O and

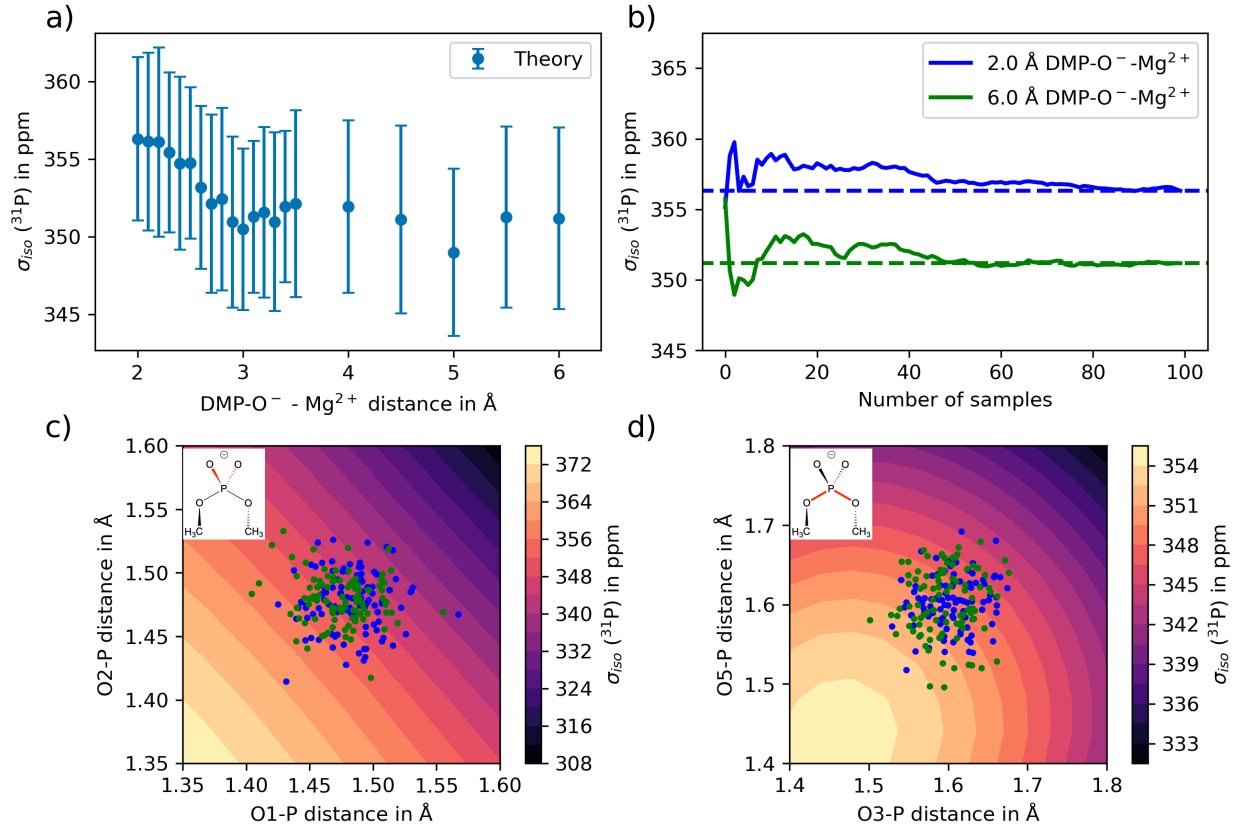


Figure 3: (a) Simulated isotropic ^{31}P shielding constants $\sigma_{iso}(^{31}\text{P})$ as a function of DMP $^-$ - Mg $^{2+}$ separation. Averages (dots) over sampled 100 configurations are shown together with the standard deviation (bars). Configurations taken from umbrella sampling in the range 2.00 Å to 6.00 Å (2100 simulations total) consider a 4.5 Å hydration shell (basis: pCVTZ/pVDZ). (b) Cumulative average of $\sigma_{iso}(^{31}\text{P})$ over 100 configurations for two DMP $^-$ - Mg $^{2+}$ separations (2 Å and 6.00 Å). (c) 2D surface of $\sigma_{iso}(^{31}\text{P})$ for the variation of O1/O2-P bond lengths (constant O3/O5-P distance: 1.60 Å). Sampled O1/O2-P bond lengths in umbrella sampling MD simulations are indicated with blue (DMP $^-$ - Mg $^{2+}$ separation: 2.00 Å) and green dots (DMP $^-$ - Mg $^{2+}$ separation: 6.00 Å), respectively. (d) 2D surface of $\sigma_{iso}(^{31}\text{P})$ for the variation of O3/O5-P bond lengths (constant O1/O2-P distance: 1.48 Å). Sampled O3/O5-P bond lengths in umbrella sampling MD simulations are indicated with blue (DMP $^-$ - Mg $^{2+}$ separation: 2.00 Å) and green dots (DMP $^-$ - Mg $^{2+}$ separation: 6.00 Å), respectively.

P-O bonds show oscillatory dynamics with characteristic frequencies in the 800–1250 cm^{−1} range,⁴⁰ corresponding to a timescale of a few tens of femtoseconds, the configurational sampling of instantaneous DMP[−] geometries induces a distributional width of $\sigma_{iso}(^{31}\text{P})$ on the order of 15–20 ppm.

The pronounced sensitivity of $\sigma_{iso}(^{31}\text{P})$ on the DMP[−] bond lengths arises from their the strong impact on the electron density of the PO₂ group and thus shielding properties of the ³¹P nuclear spin. Short O1/O2-P and O3/O5-P bond lengths lead to an increase of electron density on the PO₂ group, inducing a higher chemical shielding. As the negative charge density is primarily located on the non-bridging O1/O2-P moiety, respective bond lengths show a stronger dependence than O3/O5-P bond lengths. In comparison, angular distortions of the phosphate tetrahedron and dihedral angle displacements have a minor effect on electron density distribution of the PO₂ group and thus change of shielding properties of ³¹P.⁶⁸

Geometric mapping of isotropic ³¹P shielding constants $\sigma_{iso}(^{31}\text{P})$ Utilizing the strong geometric dependence, we aimed to establish a predictive mapping of ab initio simulated $\sigma_{iso}(^{31}\text{P})$ from geometrical parameters. For this purpose we evaluated the instantaneous O1/O2-P and O3/O5-P bond lengths of DMP[−] in MD simulations and predict $\sigma_{iso}(^{31}\text{P})$ from the 4D-coordinate map $\sigma_{iso}^{pred}(^{31}\text{P})(r_{O1-P}, r_{O2-P}, r_{O3-P}, r_{O5-P})$ (2D-surface maps are shown in Figs. 3,c-d). Predictions are then initially compared to ab initio simulated $\sigma_{iso}(^{31}\text{P})$ for the instantaneous geometry of DMP[−] in the gas phase. Figure 4,a shows the excellent correlation of this approach ($R = 0.92$, slope = 1.02), justifying the reduced dimensional mapping procedure from bond lengths and underscoring the minor role of tetrahedral and dihedral angels of DMP[−] for details of $\sigma_{iso}(^{31}\text{P})$. Note that the error in *y*-crossing (-4.04 ppm) closely reflects the uncertainty introduced via the angular O-P-O coordinate.

In a second step, we partitioned the configurational ensemble sampled in MD simulations into DMP[−] - Mg²⁺ CIP structures and free DMP[−]. For both sub-ensembles we evaluated

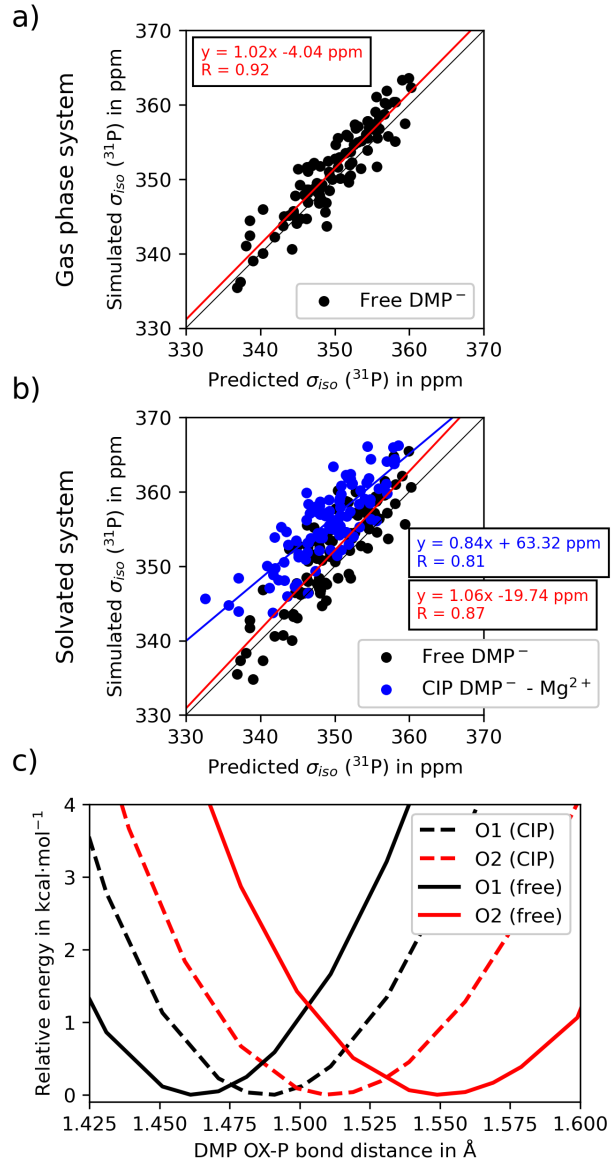


Figure 4: Geometric mapping of isotropic ^{31}P shielding constants $\sigma_{iso}(^{31}\text{P})$. (a) Correlation of ab initio simulated and predicted $\sigma_{iso}(^{31}\text{P})$ using O1/O2-P and O3/O5-P bond lengths parameters for isolated DMP $^-$ shown together with the linear regression (red). (b) Correlation of ab initio simulated and predicted $\sigma_{iso}(^{31}\text{P})$ for free DMP $^-$ in a 4.5 Å solvation shell and DMP $^-$ - Mg $^{2+}$ CIP structures using O1/O2-P and O3/O5-P bond lengths parameters. Red - linear regression of DMP $^-$ data points and blue - linear regression of CIP data points. (c) CIP-induced changes of bond lengths in hydration geometries of a DMP $^-$ - Mg $^{2+}$ CIP. Shown are scans of the O1-P and O2-P bond lengths in the DMP $^-$ - Mg $^{2+}$ CIP structure (dashed) and the equivalent DMP $^-$ solvation structure without the Mg $^{2+}$ ion, evaluating the direct impact of the ion on bond length only.

$\sigma_{iso}(^{31}\text{P})$ on the ab initio level of theory, accounting for the hydration shell up to 4.5 Å, thus accounting for the polarization of DMP^- by the hydration shell (cf. Fig. 2,a) and interactions with the bivalent Mg^{2+} counter ion (cf. Fig. 3,a). The ab initio simulated $\sigma_{iso}(^{31}\text{P})$ of $\text{DMP}^- \times N(\text{H}_2\text{O})$ w./w.o. Mg^{2+} were then compared to the predictions from geometric bond-length parameters (Fig. 4,b). Compared to the mapping of the constituent gas-phase geometries (Fig. 4,a), the correlation for both sub-ensembles is reduced. Nevertheless, when comparing both sub-ensembles, it becomes apparent that for free DMP^- the correlation of predicted and ab initio simulated ^{31}P σ_{iso} is only slightly reduced ($R = 92$ vs. 87), also the slope of 1.06 is reasonable. We interpret this finding that net influence of the full hydration environment of DMP^- on $\sigma_{iso}(^{31}\text{P})$ is minor. The spherical hydration shell to some extent polarizes the charge density of the PO_2 group but only has a moderate impact on the shielding properties. Indeed, when comparing $\sigma_{iso}(^{31}\text{P})$ simulated for DMP^- in water and free DMP^- in vacuum, respective isotropic ^{31}P shielding constants only differ by 0.7 ppm (cf. Table 4). For comparison, the geometric mapping prediction yields an error of 1.4 ppm.

Comparing the CIP and the free DMP^- sub-ensembles, we find that for the former correlation coefficients are further reduced ($R = 81$ vs. 87) and linear regression yields a largely modified slope of 0.84 with a substantially upshifted y-axis zero-crossing (63.3 ppm). Thus, $\sigma_{iso}(^{31}\text{P})$ of the CIP sub-ensemble statistically occur shielded compared to the free DMP^- counterpart. The statistical analysis demonstrates that the predominant interaction leading to a breakdown of the geometric correlation of $\sigma_{iso}(^{31}\text{P})$ arises from ion pairing with Mg^{2+} . ^{31}P NMR is thus suggested to be particularly sensitive to the formation of CIP.

The sensitivity towards CIP is further corroborated by comparing $\sigma_{iso}(^{31}\text{P})$ simulated for free DMP^- and $\text{DMP}^- - \text{Mg}^{2+}$ CIP in water and and vacuum. Both show a shift $\Delta\sigma_{iso}(^{31}\text{P})$ by -3.9 ppm and -3.5 ppm, respectively (cf. Table 4). A similar effect is found for $\text{DMP}^- - \text{Ca}^{2+}$ CIP, where the shift of $\sigma_{iso}(^{31}\text{P})$ in water is even more pronounced ($\Delta\sigma_{iso}(^{31}\text{P}) = -7.6$ ppm, Table 4). Part of the larger shift for Ca^{2+} is ascribed to the solvation shell that is more pronounced as compared to Mg^{2+} (blue line in Fig. 2,a).

Table 4: Simulated ($\sigma_{iso}^{sim}(^{31}P)$) and predicted ($\sigma_{iso}^{pred}(^{31}P)$) isotropic ^{31}P shielding constants in DMP^- : ab initio simulated $\sigma_{iso}^{sim}(^{31}P)$ are calculated on the GIAO-DF-LMP2 level of theory with a full pCVTZ basis set and a solvation shell of 4.5 Å.

System	$\sigma_{iso}^{sim}(^{31}P)$ / ppm	$\sigma_{iso}^{pred}(^{31}P)$ / ppm
Free DMP^- in water	351.9	-
Free DMP^- in vacuum	351.2	349.8
CIP DMP^- - Mg^{2+} in water	355.8	-
CIP DMP^- - Mg^{2+} in vacuum	354.7	352.8
CIP DMP^- - Ca^{2+} in water	359.5	-
CIP DMP^- - Ca^{2+} in vacuum	354.3	357.9

We ascribe the width of the $\sigma_{iso}(^{31}P)$ distributions and the shift of mean along the 1D-reaction coordinate of CIP DMP^- - Mg^{2+} CIP formation (cf. Fig. 3,a) to two main structural factors, (i) the stochastic sampling of O-P bond lengths and (ii) CIP formation. The simulations show that a Gaussian inhomogeneity on the order of 10–20 ppm arises from the sampling of instantaneous DMP^- geometries, dominated by the distribution of P-O bond lengths. The width of the distributions is largely independent of details of the reaction coordinate of CIP formation. In contrast the increased shielding, reflected in the mean of simulated $\sigma_{iso}(^{31}P)$ for short (< 2.5 Å) DMP^- - Mg^{2+} distances arises from the direct interaction with Mg^{2+} ions upon CIP formation. Structurally, CIP formation is related to the replacement of a H_2O molecule in the octahedral first solvation shell of the ion by one of the non-bridging oxygen atoms O1/O2 of DMP^- (cf. Fig. 1,a).

As $\sigma_{iso}(^{31}P)$ is highly sensitive to the local electronic environment and geometry of phosphorus atoms, the increased shielding of the ^{31}P spin in CIP is potentially induced by the geometric details, like bond length changes of the PO_2 group upon CIP formation, a change of electron density via polarization of the PO_2 group by the adjacent Mg^{2+} and/or electron density changes due to charge transfer between DMP^- and Mg^{2+} . We aimed to disentangle the origin of the shielding in DMP^- - Mg^{2+} CIP by evaluating the CIP-induced changes of bond lengths in hydration geometries of the DMP^- - Mg^{2+} CIP (Fig.4,c). Further we

monitored changes of net atomic charges of solvated DMP^- and solvated $\text{DMP}^- - \text{Mg}^{2+}$ CIP (Table 2). Fig.4,c shows the scan of O1-P and O2-P bond length in the $\text{DMP}^- - \text{Mg}^{2+}$ CIP structure with and without Mg^{2+} , preserving the hydration geometry and only evaluating the direct impact of the ion. Due to the asymmetric hydration environment in neither geometry O1-P and O2-P bond lengths are equivalent. Nevertheless, bond length changes upon addition or removal of the Mg^{2+} ion are imprinted in mirror direction on the PO_2 , i.e., a CIP-induced contraction of O2-P is accompanied by an elongation of O1-P by nearly the same amount. Thus, the mapping of changes of O1-P and O2-P bond lengths to changes of $\sigma_{iso}^{(31\text{P})}$ (Fig.3,c) suggests that the effects on $\sigma_{iso}^{(31\text{P})}$ are nearly cancelled.

To the contrary, the analysis of atomic partial charge differences Δq demonstrates the re-polarization and charge transfer upon CIP formation. On average, the high charge density of Mg^{2+} leads to a charge transfer on the order of 0.13 e^- between DMP^- and Mg^{2+} ($\text{DMP}^{0.87-} - \text{Mg}^{1.87+}$). The non-bridging oxygen O1 in contact with Mg^{2+} acquires substantial positive polarization ($\Delta q_{O1} = 0.138\text{ e}^-$) that, besides charge transfer with Mg^{2+} , is compensated by minor charge differences on bridging O3/O5 oxygen atoms and methyl groups. Thus, a net flux of charge from the non-bridging backbone region to the O1-P bond increases the charge density on the phosphorus atom ($\Delta q_P = -0.014\text{ e}^-$), correlating with increased shielding, while non-bridging O1 and O2 oxygen atoms acquire substantial charge asymmetry ($\Delta q_{O2} = -0.0004\text{ e}^-$). Notably, charge density changes on the phosphorus atom are more pronounced for Ca^{2+} ($\Delta q_P = -0.18\text{ e}^-$). In summary our results suggest that the predominant interaction for the increased shielding of $\sigma_{iso}^{(31\text{P})}$ is charge transfer, accompanied by a re-polarization of the PO_2 group, inducing a net increase of electron density at the position of the phosphorus atom, while geometric effects on $\sigma_{iso}^{(31\text{P})}$ are minor.

Quantitative analysis of contact ion pair formation

Comparing the experimentally observed $\Delta\delta_{iso}(^{31}\text{P})$ on order of -2 ppm with simulated chemical shift differences $\Delta\delta^{sim}(^{31}\text{P})$ of free DMP and $\text{DMP}^- - \text{Mg}^{2+}$ CIP

$$\begin{aligned}\Delta\delta^{sim}(^{31}\text{P}) &= \sigma_{iso}^{Ref}(^{31}\text{P}) - \sigma_{iso}(^{31}\text{P})[\text{CIP}] - (\sigma_{iso}^{Ref}(^{31}\text{P}) - \sigma_{iso}(^{31}\text{P})[\text{FreeDMP}^-]) \\ &= \sigma_{iso}(^{31}\text{P})[\text{FreeDMP}^-] - \sigma_{iso}(^{31}\text{P})[\text{CIP}],\end{aligned}\quad (2)$$

translates into $\Delta\delta^{sim}(^{31}\text{P})$ with same sign as in the experiment, corresponding to a shielding of the ^{31}P nucleus in CIP (Table 4). Nevertheless, a substantial discrepancy persists when comparing the amplitude of the chemical shift differences $\Delta\delta_{iso}(^{31}\text{P})$ and $\Delta\delta^{sim}(^{31}\text{P})$, that is on the order of $\Delta\delta^{sim}(^{31}\text{P}) \approx -3.9$ ppm in simulations.

Assuming a two component model, where deviations $\Delta\delta_{iso}(^{31}\text{P})$ relative to free DMP $^-$ (0 eq. Mg^{2+} , cf. Fig 1) are induced by $\text{DMP}^- - \text{Mg}^{2+}$ CIP, i.e., subsuming the population of fully solvated species SSIP with free DMP $^-$, the observed $\Delta\delta_{iso}(^{31}\text{P})$ is only influenced by the relative population $c[\text{CIP}]$ induced by the bimolecular formation of the $\text{DMP}^- - \text{Mg}^{2+}$ CIP species:

$$\Delta\delta_{iso}(^{31}\text{P}) \propto c[\text{CIP}], c[\text{FreeDMP}^-]. \quad (3)$$

Taking now the chemical shift values from simulations to characterize $\Delta\delta_{iso}^{max}(^{31}\text{P}) = \Delta\delta^{sim}(^{31}\text{P})$, the maximal amplitude $\Delta\delta_{iso}^{max}(^{31}\text{P}) = -3.9$ ppm correlates to a CIP formation of 100 %. The relative fractional population $X[\text{CIP}] = n[\text{CIP}] / n[\text{DMP}^-]$ can then be expressed as^{31,69}

$$X[\text{CIP}] = \frac{\delta_{iso}(^{31}\text{P})[x \text{ eq. } \text{Mg}^{2+}] - \delta_{iso}(^{31}\text{P})[0 \text{ eq. } \text{Mg}^{2+}]}{\Delta\delta_{iso}^{max}(^{31}\text{P})}. \quad (4)$$

Figure 5,a presents the relative fractional population $X[\text{CIP}]$, derived from eq. 4, as a function of Mg^{2+} content and temperature. The model suggests a variation of $X[\text{CIP}]$ in the range 0–60 % for up to 25 eq. Mg^{2+} , i.e., saturation limit is not achieved in the investigated ion concentration range. Temperature variation in the range 17–35 °C increases $X[\text{CIP}]$ by

about 10 % for 10 eq. Mg^{2+} and by about 15 % for 25 eq. Mg^{2+} . Comparing the ^{31}P -NMR results for 10 eq. Mg^{2+} (298 K, $X[CIP] = 28\%$) with values derived from infrared and 2D-infrared spectroscopy²⁰ (black line and green bars in Fig. 5,a), the relative populations are in good agreement.

The determination of the relative CIP population $X[CIP]$ depends on the maximal amplitude from ab initio simulations $\Delta\delta_{iso}^{max}(^{31}P) = \Delta\delta^{sim}(^{31}P)$. To explore the sensitivity of our results, we investigated the dependence of $\Delta\delta^{sim}(^{31}P)$ on basis set size. As $\Delta\delta^{sim}(^{31}P)$ are very similar for DMP^- and $DMP^- - Mg^{2+}$ CIP in the gas phase and in water (−3.9 ppm and −3.5 ppm, respectively; Table 4), we explored the convergence of $\Delta\delta^{sim}(^{31}P)$ up to quintuple zeta basis sets in gas phase simulations (Fig. 5,b). We find that convergence for the ionic species is slow and deviations are on the order of 0.6–0.8 ppm, corresponding to a 17.1–22.9 % uncertainty in the relative population $X[CIP]$. For aqueous DMP^- and $DMP^- - Mg^{2+}$ CIP we find a reduced sensitivity on basis set (up to quadruple zeta), suggesting a faster convergence of $\Delta\delta^{sim}(^{31}P)$ within 0.2 ppm (red star in Fig. 5,b; corresponding uncertainty in $X[CIP]$: 5–10 %)].

For comparison, Fig. 5,c depicts $\delta_{iso}(^{31}P)$ for varying Ca^{2+} concentrations, for which $\Delta\delta_{iso}(^{31}P)$ spans a range of −1.4 ppm. Combining these values with the chemical shift amplitude $\Delta\delta^{sim}(^{31}P) = -7.6$ ppm in $DMP^- - Ca^{2+}$ CIP (see Table 4) suggests a reduced population $X[CIP]$ for Ca^{2+} compared to Mg^{2+} . For 10 eq. Ca^{2+} the derived population $X[CIP] = 0.1$ is slightly outside the 12–30 % range suggested by infrared and 2D-infrared spectroscopy²⁰ (green bars in Fig. 5,c). Again, NMR derived concentrations more closely reflect the lower bound derived from infrared experiments.

Discussion

Experimentally, the increase in concentration of the bivalent counterion Mg^{2+} in a range [0–25] eq. leads to a chnage of chemical shift $\Delta\delta_{iso}(^{31}P) = -2.07$ ppm in DMP^- , i.e., a shielding

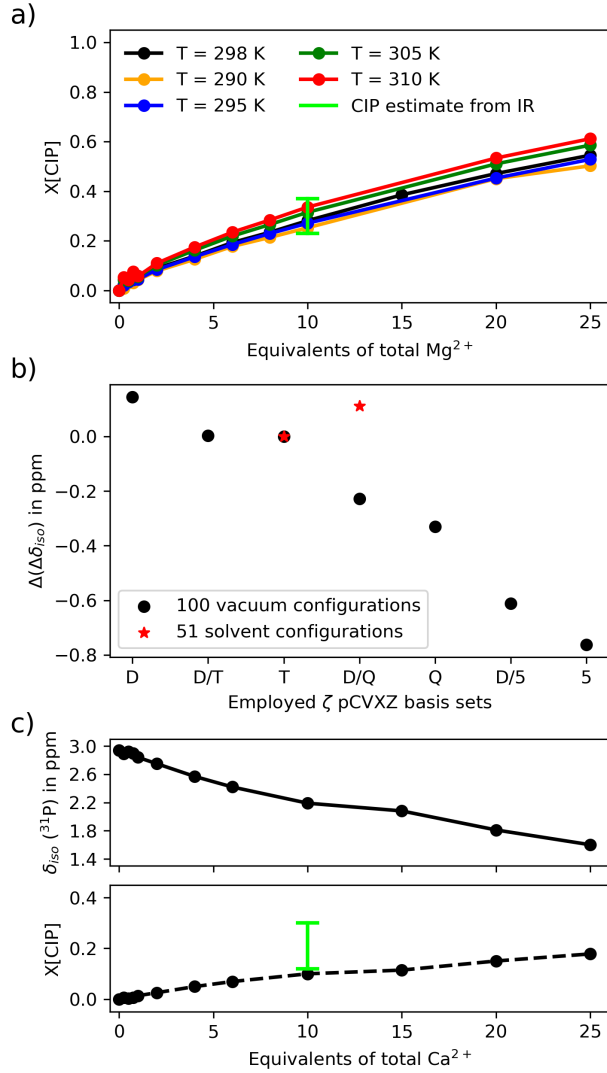


Figure 5: (a) Relative CIP population $X[CIP]$ (Eq. 4) for varying Mg²⁺ content and temperature in comparison to results from infrared spectroscopy²⁰ (green bars). (b) Basis set dependence of amplitude of simulated chemical shift differences $\Delta\delta_{iso}^{max}(^{31}P)$ of free DMP⁻ and DMP⁻ - Mg²⁺ CIP (gas phase simulations), red stars show $\Delta\delta_{iso}^{max}(^{31}P)$ of free DMP⁻ and DMP⁻ - Mg²⁺ CIP with water environment obtained with a pCVQZ basis set. (c) Observed chemical shifts $\delta^{(31)P}$ for varying Ca²⁺ content (298 K) and derived DMP⁻ - Ca²⁺ CIP population $X[CIP]$ (dashed line, lower panel). For comparison results derived from infrared spectroscopy are shown (green bars).

of the ^{31}P nucleus with moderate temperature dependence. The magnitude of $\Delta\delta_{iso}(^{31}\text{P})$ is comparable but reduced (-1.4 ppm) for Ca^{2+} at room temperature. Notably, for both bivalent counterions, saturation behavior is not observed, even for the highest investigated ion content. High level ab initio theory (GIAO-DF-LMP2) predicts a shielding of the ^{31}P spin in CIP by $\Delta\delta^{sim}(^{31}\text{P}) = -3.9\text{ ppm}$ and -7.6 ppm for Mg^{2+} and Ca^{2+} , respectively, that is comparable in magnitude to studies on DNA - Mg^{2+} binding using density functional theory.⁷⁰ While both theory and experiments show a shielding of the ^{31}P spin, the simulations for both ions suggest a substantially larger chemical shift amplitude $\Delta\delta^{sim}(^{31}\text{P})$ associated with CIP formation.

The observations were analyzed in a two-component model (Eq. 4), where $\delta_{iso}(^{31}\text{P})$ is determined by the average chemical shift of DMP^- and $X[\text{CIP}]$, the unknown relative fraction of DMP^- - Mg^{2+} CIP. As such, the model assumes the fast exchange of solvation species on the timescale of the experiment, leading to a single average peak $\delta^{sim}(^{31}\text{P})$ in the ^{31}P -NMR spectra (Fig 1,c). Further, fully solvated DMP^- species, i.e. SSIP and free DMP^- , are assumed to be indistinguishable in the ^{31}P -NMR experiment, which is motivated by the minor chemical shift differences of SSIP and free DMP^- in simulations (Fig. 3,a). The model reproduces two key observations: (i) the missing saturation behavior in the investigated concentration range and (ii) the moderate temperature dependence of $\delta_{iso}(^{31}\text{P})$. The relative CIP fraction $X[\text{CIP}]$ was then determined in a broad range of Mg^{2+} concentrations up to 25 eq., approaching $\approx 50 \pm 10\%$ at room temperature, where the uncertainty is estimated from the variation of the chemical shift amplitude $\Delta\delta^{sim}(^{31}\text{P})$ (Fig. 5,b).

While similar two-component models have been invoked before to describe ion induced chemical shift changes in ^{31}P NMR spectra,^{26,31} the assignment so far assumed an unspecified cationic bound species, tentatively assigned to ion pairing, without molecular distinction of the strongly interacting CIP and SSIP species. In the current work, we provide an in-depth ab initio analysis of the microscopic mechanism leading to the observed chemical shift changes associated with the molecular solvation species (CIP, SSIP and free DMP^- ,

respectively). Further the influence of the solution environment is explored in comparison to gas phase simulations. The ab initio determination of $\sigma^{iso}(^{31}P)$ strongly suggests that the ^{31}P chemical shifts of DMP^- are particularly sensitive to the formation of CIP (Fig. 3,a). Moreover, the explored concentration range is much broader than in previously reported ^{31}P -NMR experiments. Association constants derived from dielectric relaxation and ^{31}P -NMR spectroscopy agree well at low concentrations (< 2 eq.). For multiple eq. of Mg^{2+} or Ca^{2+} (>4) the ion populations derived from a fit of the amplitude $\Delta\delta_{iso}^{max}(^{31}P)$ acquire increasing uncertainty, presumably due to secondary ion hydration equilibria.⁷¹ Note that even for highest Mg^{2+} content (25 eq.), the ion concentration is about 2.2 M, i.e., enough water for the full solvation of ionic species is assured under the current experimental conditions.

The high sensitivity of ^{31}P NMR to detect CIP of DMP^- with bivalent ions Mg^{2+} and Ca^{2+} resembles findings from IR and 2D-IR spectroscopy that selectively report on contact ion pair formation with PO_2 groups.¹⁸⁻²⁰ The derived relative CIP fractions $X[CIP]$ at 10 eq. of ions agree reasonably (Figs. 5,a,c). Despite these comparable analytical findings, the underlying mechanism responsible for high species sensitivity is vastly different in the two experimental techniques. The short $P-O^-...Mg^{2+}$ distance in CIP of about 2.1 Å induces a strong perturbation of the PO_2 mode potential, primarily arising from exchange repulsion interactions of the closed shell Mg^{2+} and PO_2 electron density. In the IR-spectra, this leads to a characteristic blue shift on the order of 20-30 cm^{-1} of the asymmetric PO_2 stretching vibration, compared to fully solvated PO_2 groups.^{19,20} Considering the typical linewidths of the asymmetric PO_2 stretching vibration (on the order of 30 – 70 cm^{-1} in DNA and RNA⁷²), the CIP-induced blue shift leads to a shoulder in the IR spectra of the asymmetric PO_2 stretching vibration that can be accentuated via non-linear 2D-techniques. The lineshapes in 2D-IR spectra are characterized to a large extent by a quasi-homogeneous contribution from fast (sub-100 fs) structural fluctuations⁷³ and, on the timescale of the IR experiments (femto- to picoseconds), longer-lived structural inhomogeneities. The IR lineshapes thus mirror the population of all species and encode details of the CIP population and the hydration

environment.

In contrast, ^{31}P -NMR spectra report on changes of electron density of the PO_2 group upon CIP formation. The observation of the shielding of the ^{31}P in CIP hydration structures is a signature of the modified charge density, where the strong interaction with Mg^{2+} and Ca^{2+} leads to charge transfer on the order of 0.13 e^- between CIP constituents and a polarization of the PO_2 group that breaks the symmetry between the two non-bridging oxygen atoms. The ^{31}P relaxation rates reflect the fast motional regime (extreme narrowing limit, $\omega_0\tau_L \ll 1$) and in addition a contribution from molecular exchange events between CIP and SSIP or free DMP^- . The population weighted average chemical shift $\delta_{iso}(^{31}\text{P})$ of CIP and free DMP^- is observed for every counter ion concentration (cf. Fig. 1,c). The magnitude of $\Delta\delta_{iso}(^{31}\text{P})$ ($\approx -2\text{ ppm}$) is substantially larger than the NMR linewidths. Thus, ^{31}P -NMR spectroscopy provides in principle a higher sensitivity than IR spectroscopy at low bivalent ion concentrations. The technique further offers potential to discriminate long- and short-lived ion pair species with PO_2 groups. For example, ^{31}P NMR spectra of tRNA²⁷ show the emergence of individual lines for increasing Mg^{2+} concentration. The observed exchange broadenings with increasing Mg^{2+} concentration (Table 3) are well documented.^{74,75} Based on the calculated $\Delta\delta^{sim}(^{31}\text{P})$, the exchange rate for which coalescence of the resonances lines of free DMP^- and CIP is expected is about 2800 s^{-1} , corresponding to a lifetime of $350\text{ }\mu\text{s}$ of the CIP. Estimates of the exchange rate have placed a lower limit on the exchange time scale of $1\text{ }\mu\text{s}$.¹⁰

The theoretical assignment of the observed chemical shift changes $\Delta\delta_{iso}(^{31}\text{P})$ to CIP formation is further corroborated by ^{31}P -NMR experiments with Zn^{2+} , Cd^{2+} , $\text{Co}(\text{NH}_3)_6^{3+}$ and Na^+ counter ions (summarized in Table 3). Among the latter, only Zn^{2+} induces a comparable shift of $\delta_{iso}(^{31}\text{P})$, suggesting the formation of a substantial fraction of CIP. Severe perturbation of the ^{31}P -NMR lineshape precludes quantitative analysis for $> 0.1\text{ eq}$. While for Na^+ the minor deshielding ($\Delta\delta_{iso}(^{31}\text{P}) = 0.07\text{ ppm}$) is well documented and correlates with the minor tendency of $\text{DMP}^- - \text{Na}^+$ CIP formation suggested by IR spectroscopy,²⁰

the absence of a substantial $\Delta\delta_{iso}(^{31}\text{P})$ for $\text{Co}(\text{NH}_3)_6^{3+}$ strongly supports the notion that observed ^{31}P chemical shift changes are induced by CIP formation. Despite the high charge density of Co^{3+} , $\text{Co}(\text{NH}_3)_6^{3+}$ is well established to interact via outer sphere contacts only⁷⁶ and the ^{31}P experiments for relatively high $\text{Co}(\text{NH}_3)_6^{3+}$ content (4-10 eq.) demonstrate that outer sphere interaction of DMP^- with multivalent ions has negligible effect on $\delta_{iso}(^{31}\text{P})$. *Vice versa*, the minor $\Delta\delta_{iso}(^{31}\text{P})$ observed for Cd^{2+} is in line with explorative MD that show a spontaneous transformation of CIP into SSIP and free DMP^- on a < 100 ns timescale, suggesting a minor role of CIP in solutions of DMP^- and Cd^{2+} . NMR should thus be considered an effective short range reporter with particular CIP sensitivity, providing a local view of the electrostatics of PO_2 groups.

In the simulations, the width of the $\sigma_{iso}(^{31}\text{P})$ distributions (standard deviation ≈ 12 ppm) is much broader than the linewidth of the ^{31}P -NMR spectra and largely independent of the DMP^- - ion separation (Fig. 3). As DMP^- - Mg^{2+} geometries are sampled from MD simulations, the statistical sampling of P-O bond lengths is directly reflected in the width of simulated $\delta(^{31}\text{P})$ distributions. Due to the particular short-range sensitivity of $\sigma_{iso}(^{31}\text{P})$ to variations of the local charge density, the statistical sampling of P-O bond lengths was shown to be the dominant contribution to the distributional width. Exploiting this relation allowed us to develop a low-dimensional geometric mapping procedure of $\sigma_{iso}(^{31}\text{P})$ of DMP^- that utilizes the instantaneous P-O bond lengths of the MD trajectory (Fig. 4). The mapping approach provides quantitative insight into the distributional widths, allows to de-noise the real-time data of MD simulations for the determination of $\delta_{iso}(^{31}\text{P})$ in close comparison to NMR experiments and suggests that contributions from O-P-O angles and backbone conformation are minor.⁶⁸ Moreover the mapping approach establishes a statistical foundation for $\Delta\delta_{iso}(^{31}\text{P})$ induced by CIP geometries that is encoded in the shift of the mean the distributions of $\delta_{iso}(^{31}\text{P})$. Similar strong dependence of $\delta(^{31}\text{P})$ on P-O bond lengths was previously reported from NMR spectroscopy of crystalline samples.⁷⁷

Utilizing $\Delta\delta_{iso}^{max}(^{31}\text{P}) = \Delta\delta_{iso}^{sim}(^{31}\text{P})$ in a two-component analysis of contact and fully

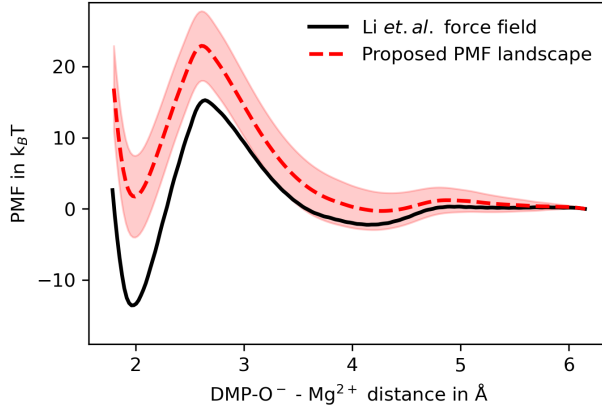


Figure 6: Relative stability of CIP and SSIP in solution. Minima of the CIP and SSIP species in the potential of mean force (PMF) determined by the 12-6-4 parametrization of intermolecular interactions by Li *et al.*^{37,49} (black) and from boundary conditions imposed on the relative population $X[CIP]$ derived in the current study (red dashed).

solvated DMP^- species, allows to establish the relative population $X[CIP]$ of contact ion pairs, that form a minor species at low ion content (< 10 eq.) and room temperature ($X[CIP] = 28\%$). Knowledge of the relative population $X[CIP]$ places boundary conditions on the relative stability of CIP and SSIP in solution (Fig. 6). Specifically, the free energy of SSIP or free DMP^- solvation species are required to be more stable than the minimum of the CIP species in the potential of mean force (PMF) and the moderate temperature dependence establishes that both minima are energetically close within a few $k_B T$. In contrast, common fixed-charge force fields^{37,49} yield CIP structures that are substantially more stable than SSIP and free DMP^- (cf. Fig. 6, black line), with the tendency of overbinding to the phosphate groups of DNA and RNA. Recent investigations on DMP^- - ion interactions²⁴ indicate that the original parametrization of the polarizable amoeba force field overestimates Mg^{2+} and Ca^{2+} binding. The results of Puyo-Fourtine *et al.*^{37,49} further suggest that force fields with overall reasonable ion binding free energies tend to underestimate CIP population in comparison to 2D-IR experimental estimates, indicating an over-stabilization of SSIP.

Our results shed light on the relative driving force of bivalent ions Mg^{2+} and Ca^{2+} to form CIP with the PO_2 group. Results from RISM theory suggest a preference of Ca^{2+} to form CIP in complex RNA structures.⁴² In the DMP^- model system, experimental and

in-depth simulations of the ^{31}P chemical shifts allowed us to firmly establish that at given concentration Mg^{2+} forms about twice as much CIP as Ca^{2+} , in agreement with findings from IR spectroscopy.²⁰ Concerning the primary PO_2^- - ion interactions, hardness of the ion and the properties of the $\text{I}^{2+}(\text{H}_2\text{O})_N$ solvation shell are the decisive factors for CIP formation. In particular, for $\text{Mg}^{2+}(\text{H}_2\text{O})_6$, the geometric constraints and desolvation of the first octahedral solvation shell around the ion introduces an substantial energetic penalty that destabilizes the CIP species relative to the SSIP species. Our results establish the microscopic origin of ^{31}P chemical shifts induced by the bare electrostatic interaction of DMP^- and bivalent counter ions, establishing a reference to quantify secondary interactions in the more complex hydration geometries of DNA and RNA.⁷²

Conclusions

Through the combination of NMR experiments and in-depth ab initio simulations of the ^{31}P chemical shift of DMP^- in aqueous solution, a model system of the DNA or RNA sugar-phosphate backbone, we have established the origin for the shielding of the ^{31}P spin upon addition of the bivalent ions Mg^{2+} and Ca^{2+} . Specifically, electronic effects arising from the formation of $\text{DMP}^- - \text{I}^{2+}$ CIP structures ($\text{I} = \text{Mg, Ca}$) are distinguished from intramolecular geometric distortions of bridging and non-bridging P-O bond lengths of the phosphate group. A low-dimensional geometric mapping procedure allows us to quantitatively describe the width of $\sigma_{iso}(^{31}\text{P})$ distributions, establishing a -3.9 ppm amplitude of ^{31}P chemical shift change ascribed to CIP formation with Mg^{2+} . Such microscopic values explain the experimental ^{31}P -NMR spectra in a vast concentration and temperature range. The data suggest that CIP are a minor species at low Mg^{2+} concentrations and a relative CIP population $X[\text{CIP}]$ approaching 50 % only occurs for large Mg^{2+} ion excess. Despite a larger ^{31}P chemical shift amplitude (-7.6 ppm), Ca^{2+} has a lower tendency of CIP formation. The derived CIP populations serve as benchmark for future force field optimization and refinement.

Acknowledgement

This research has received funding from the Deutsche Forschungsgemeinschaft (DFG) [SFB1309-C09, project number 325871075]. This work was funded by the DFG through the Cluster of Excellence *e*-conversion [Grant No. EXC2089/2-390776260, BPF] and the Emmy Noether program (project number 394455587 to AKS). We thank Peter Dowling for synthesis of the hexaamminecobalt(III) chloride. The authors acknowledge the computational and data resources provided by the Leibniz Supercomputing Centre (www.lrz.de).

References

- (1) Wong, G. C.; Pollack, L. Electrostatics of Strongly Charged Biological Polymers: Ion-Mediated Interactions and Self-Organization in Nucleic Acids and Proteins. *Annual Review of Physical Chemistry* **2010**, *61*, 171–189.
- (2) Lipfert, J.; Doniach, S.; Das, R.; Herschlag, D. Understanding Nucleic Acid–Ion Interactions. *Annual Review of Biochemistry* **2014**, *83*, 813–841.
- (3) Draper, D. E.; Grilley, D.; Soto, A. M. Ions and RNA Folding. *Annual Review of Biophysics* **2005**, *34*, 221–243.
- (4) Denesyuk, N. A.; Thirumalai, D. How do metal ions direct ribozyme folding? *Nature Chemistry* **2015**, *7*, 793–801.
- (5) Cate, J. H.; Hanna, R. L.; Doudna, J. A. A magnesium ion core at the heart of a ribozyme domain. *Nature Structural Biology* **1997**, *4*, 553–558.
- (6) Inoue, A.; Takagi, Y.; Taira, K. Importance in catalysis of a magnesium ion with very low affinity for a hammerhead ribozyme. *Nucleic Acids Research* **2004**, *32*, 4217–4223.
- (7) Schnabl, J.; Sigel, R. K. Controlling ribozyme activity by metal ions. *Current Opinion in*

Chemical Biology **2010**, *14*, 269–275, Biocatalysis and Biotransformation/Bioinorganic Chemistry.

- (8) Laage, D.; Elsaesser, T.; Hynes, J. T. Water Dynamics in the Hydration Shells of Biomolecules. *Chem. Rev.* **2017**, *117*, 13599–13634.
- (9) Fingerhut, B. P. The mutual interactions of RNA, counterions and water – quantifying the electrostatics at the phosphate–water interface. *Chem. Commun.* **2021**, *57*, 12880–12897.
- (10) Freisinger, E.; Sigel, R. K. From nucleotides to ribozymes—A comparison of their metal ion binding properties. *Coordination Chemistry Reviews* **2007**, *251*, 1834–1851, 37th International Conference on Coordination Chemistry, Cape Town, South Africa.
- (11) Bai, Y.; Greenfeld, M.; et al. D. Herschlag Quantitative and comprehensive decomposition of the ion atmosphere around nucleic acids. *Journal of the American Chemical Society* **2007**, *129*, 14070–14079.
- (12) Trachman, I., Robert J.; Draper, D. E. Divalent ion competition reveals reorganization of an RNA ion atmosphere upon folding. *Nucleic Acids Research* **2017**, *45*, 4733–4742.
- (13) Jacobson, D. R.; Saleh, O. A. Counting the ions surrounding nucleic acids. *Nucleic Acids Research* **2016**, *45*, 1596–1605.
- (14) Pabit, S. A.; Meisburger, S. P.; Li, L.; Blose, J. M.; Jones, C. D.; Pollack, L. Counting Ions around DNA with Anomalous Small-Angle X-ray Scattering. *Journal of the American Chemical Society* **2010**, *132*, 16336–16344.
- (15) Gebala, M.; Herschlag, D. Quantitative Studies of an RNA Duplex Electrostatics by Ion Counting. *Biophysical Journal* **2019**, *117*, 1116–1124.
- (16) Pollack, L. SAXS Studies of Ion–Nucleic Acid Interactions. *Annual Review of Biophysics* **2011**, *40*, 225–242.

(17) Fingerhut, B. P.; Schauss, J.; Kundu, A.; Elsaesser, T. Contact pairs of RNA with magnesium ions-electrostatics beyond the Poisson-Boltzmann equation. *Biophysical Journal* **2021**, *120*, 5322–5332.

(18) Schauss, J.; Kundu, A.; Fingerhut, B. P.; Elsaesser, T. Magnesium Contact Ions Stabilize the Tertiary Structure of Transfer RNA: Electrostatics Mapped by Two-Dimensional Infrared Spectra and Theoretical Simulations. *The Journal of Physical Chemistry B* **2021**, *125*, 740–747, PMID: 33284610.

(19) Schauss, J.; Dahms, F.; Fingerhut, B. P.; Elsaesser, T. Phosphate–Magnesium Ion Interactions in Water Probed by Ultrafast Two-Dimensional Infrared Spectroscopy. *The Journal of Physical Chemistry Letters* **2019**, *10*, 238–243.

(20) Schauss, J.; Kundu, A.; Fingerhut, B. P.; Elsaesser, T. Contact Ion Pairs of Phosphate Groups in Water: Two-Dimensional Infrared Spectroscopy of Dimethyl Phosphate and ab Initio Simulations. *The Journal of Physical Chemistry Letters* **2019**, *10*, 6281–6286, PMID: 31560211.

(21) Fingerhut, B. P.; Schauss, J.; Kundu, A.; Elsaesser, T. Aqueous Contact Ion Pairs of Phosphate Groups with Na^+ , Ca^{2+} and Mg^{2+} – Structural Discrimination by Femtosecond Infrared Spectroscopy and Molecular Dynamics Simulations. *Zeitschrift für Physikalische Chemie* **2020**, *234*, 1453–1474.

(22) Florián, J.; Štrajbl, M.; Warshel, A. Conformational Flexibility of Phosphate, Phosphonate, and Phosphorothioate Methyl Esters in Aqueous Solution. *Journal of the American Chemical Society* **1998**, *120*, 7959–7966.

(23) Fingerhut, B. P.; Costard, R.; Elsaesser, T. Predominance of short range Coulomb forces in phosphate-water interactions—a theoretical analysis. *The Journal of Chemical Physics* **2016**, *145*, 115101.

(24) Puyo-Fourtine, J.; Juillé, M.; Hénin, J.; Clavaguéra, C.; Duboué-Dijon, E. Consistent Picture of Phosphate–Divalent Cation Binding from Models with Implicit and Explicit Electronic Polarization. *The Journal of Physical Chemistry B* **2022**, *126*, 4022–4034, PMID: 35608554.

(25) Delgado, J. M.; Nagy, P. R.; Varma, S. Polarizable AMOEBA Model for Simulating Mg²⁺·Protein·Nucleotide Complexes. *Journal of Chemical Information and Modeling* **2024**, *64*, 378–392, PMID: 38051630.

(26) Kutus, B.; Wagner, K.; Wagner, M.; Hunger, J. Ion-pairing equilibria and kinetics of dimethyl phosphate: A model for counter-ion binding to the phosphate backbone of nucleic acids. *Journal of Molecular Liquids* **2022**, *363*, 119868.

(27) Guéron, M.; Shulman, R. G. ³¹P magnetic resonance of tRNA. *Proceedings of the National Academy of Sciences* **1975**, *72*, 3482–3485.

(28) Tran-Dinh, S.; Neumann, J. A ³¹P - NMR study of the interaction of Mg²⁺ ions with nucleoside diphosphates. *Nucleic Acids Research* **1977**, *4*, 397–403.

(29) TRAN-DINH, S.; ROUX, M. A Phosphorus-Magnetic-Resonance Study of the Interaction of Mg²⁺ with Adenyl-5'-yl Imidodiphosphate. *European Journal of Biochemistry* **1977**, *76*, 245–249.

(30) Rose, D. M.; Bleam, M. L.; Record, M. T.; Bryant, R. G. ²⁵Mg NMR in DNA solutions: Dominance of site binding effects. *Proceedings of the National Academy of Sciences* **1980**, *77*, 6289–6292.

(31) Haake, P.; Prigodich, R. V. Method for determination of phosphate anion-cation association constants from phosphorus-31 chemical shifts. *Inorganic Chemistry* **1984**, *23*, 457–462.

(32) Donghi, D.; Sigel, R. K. O. In *Ribozymes: Methods and Protocols*; Hartig, J. S., Ed.; Humana Press: Totowa, NJ, 2012; pp 253–273.

(33) Marino, J. P.; Schwalbe, H.; Anklin, C.; Bermel, W.; Crothers, D. M.; Griesinger, C. Three-Dimensional Triple-Resonance ^1H , ^{13}C , ^{31}P Experiment: Sequential Through-Bond Correlation of Ribose Protons and Intervening Phosphorus along the RNA Oligonucleotide Backbone. *Journal of the American Chemical Society* **1994**, *116*, 6472–6473.

(34) Fürtig, B.; Richter, C.; Wöhnert, J.; Schwalbe, H. NMR Spectroscopy of RNA. *Chem-BioChem* **2003**, *4*, 936–962.

(35) Szántó, J. K.; Dietschreit, J. C. B.; Shein, M.; Schütz, A. K.; Ochsenfeld, C. Systematic QM/MM Study for Predicting ^{31}P NMR Chemical Shifts of Adenosine Nucleotides in Solution and Stages of ATP Hydrolysis in a Protein Environment. *Journal of Chemical Theory and Computation* **2024**, *20*, 2433–2444, PMID: 38497488.

(36) Shein, M.; Hitzenberger, M.; Cheng, T.; Rout, S.; Leitl, K.; Sato, Y.; Zacharias, M.; Sakata, E.; Schütz, A. K. Characterizing ATP processing by the AAA+ protein p97 at the atomic level. *Nature Chemistry* **2024**, *16*, 363–372.

(37) Li, P.; Roberts, B. P.; Chakravorty, D. K.; Merz, K. M. J. Rational Design of Particle Mesh Ewald Compatible Lennard-Jones Parameters for +2 Metal Cations in Explicit Solvent. *Journal of Chemical Theory and Computation* **2013**, *9*, 2733–2748, PMID: 23914143.

(38) Xu, H.-T.; Zhang, N.; Li, M.-R.; Zhang, F.-S. Comparison of the ionic effects of Ca^{2+} and Mg^{2+} on nucleic acids in liquids. *Journal of Molecular Liquids* **2021**, *344*, 117781.

(39) Koca Fındık, B.; Jafari, M.; Song, L. F.; Li, Z.; Aviyente, V.; Merz, K. M. J. Binding of Phosphate Species to Ca^{2+} and Mg^{2+} in Aqueous Solution. *Journal of Chemical Theory and Computation* **2024**, *20*, 4298–4307, PMID: 38718258.

(40) Costard, R.; Tyborski, T.; Fingerhut, B. P.; Elsaesser, T. Ultrafast phosphate hydration dynamics in bulk H₂O. *The Journal of Chemical Physics* **2015**, *142*, 212406.

(41) Kundu, A.; Fingerhut, B. P.; Elsaesser, T. Hydration structure and dynamics of phosphoric acid and its anions—Ultrafast 2D-IR spectroscopy and ab initio molecular dynamics simulations. *The Journal of Chemical Physics* **2024**, *161*, 084503.

(42) Nguyen, H. T.; Thirumalai, D. Charge Density of Cation Determines Inner versus Outer Shell Coordination to Phosphate in RNA. *The Journal of Physical Chemistry B* **2020**, *124*, 4114–4122, PMID: 32342689.

(43) Bjerrum, J.; McReynolds, J. P.; Oppegard, A. L.; Parry, R. W. *Inorganic Syntheses*; John Wiley & Sons, Ltd, 1946; pp 216–221.

(44) Hoffman, R. E.; Becker, E. D. Temperature dependence of the ¹H chemical shift of tetramethylsilane in chloroform, methanol, and dimethylsulfoxide. *Journal of Magnetic Resonance* **2005**, *176*, 87–98.

(45) Ammann, C.; Meier, P.; Merbach, A. A simple multinuclear NMR thermometer. *Journal of Magnetic Resonance (1969)* **1982**, *46*, 319–321.

(46) Case, D. A.; Cerutti, D. S.; Cruzeiro, V. W. D.; Darden, T. A.; Duke, R. E.; Ghazimirsaeed, M.; Giambasu, G. M.; Giese, T. J.; Götz, A. W.; Harris, J. A. et al. Recent Developments in Amber Biomolecular Simulations. *Journal of Chemical Information and Modeling* **2025**, *65*, 7835–7843, PMID: 40728386.

(47) Ivani, I.; Dans, P. D.; Noy, A.; Pérez, A.; Faustino, I.; Hospital, A.; Walther, J.; Andrio, P.; Goñi, R.; Balaceanu, A. et al. Parmbsc1: a refined force field for DNA simulations. *Nature Methods* **2016**, *13*, 55–58.

(48) Wang, L.-P.; Martinez, T. J.; Pande, V. S. Building Force Fields: An Automatic,

Systematic, and Reproducible Approach. *The Journal of Physical Chemistry Letters* **2014**, *5*, 1885–1891.

(49) Li, Z.; Song, L. F.; Li, P.; Merz, K. M. Systematic Parametrization of Divalent Metal Ions for the OPC3, OPC, TIP3P-FB, and TIP4P-FB Water Models. *Journal of Chemical Theory and Computation* **2020**, *16*, 4429–4442.

(50) Sengupta, A.; Li, Z.; Song, L. F.; Li, P.; Merz, K. M. Parameterization of Monovalent Ions for the OPC3, OPC, TIP3P-FB, and TIP4P-FB Water Models. *Journal of Chemical Information and Modeling* **2021**, *61*, 869–880.

(51) Case, D. A.; Aktulga, H. M.; Belfon, K.; Cerutti, D. S.; Cisneros, G. A.; Cruzeiro, V. W. D.; Forouzesh, N.; Giese, T. J.; Götz, A. W.; Gohlke, H. et al. AmberTools. *Journal of Chemical Information and Modeling* **2023**, *63*, 6183–6191, PMID: 37805934.

(52) Roe, D. R.; Cheatham, T. E. I. PTraj and CPPtraj: Software for Processing and Analysis of Molecular Dynamics Trajectory Data. *Journal of Chemical Theory and Computation* **2013**, *9*, 3084–3095, PMID: 26583988.

(53) Humphrey, W.; Dalke, A.; Schulten, K. VMD: Visual molecular dynamics. *Journal of Molecular Graphics* **1996**, *14*, 33–38.

(54) Darden, T.; York, D.; Pedersen, L. Particle mesh Ewald: An $N \cdot \log(N)$ method for Ewald sums in large systems. *The Journal of Chemical Physics* **1993**, *98*, 10089–10092.

(55) Essmann, U.; Perera, L.; Berkowitz, M. L.; Darden, T.; Lee, H.; Pedersen, L. G. A smooth particle mesh Ewald method. *The Journal of Chemical Physics* **1995**, *103*, 8577–8593.

(56) Ryckaert, J.-P.; Ciccotti, G.; Berendsen, H. J. Numerical integration of the cartesian equations of motion of a system with constraints: molecular dynamics of n-alkanes. *Journal of computational physics* **1977**, *23*, 327–341.

(57) Miyamoto, S.; Kollman, P. A. Settle: An analytical version of the SHAKE and RATTLE algorithm for rigid water models. *Journal of Computational Chemistry* **1992**, *13*, 952–962.

(58) Loncharich, R. J.; Brooks, B. R.; Pastor, R. W. Langevin dynamics of peptides: The frictional dependence of isomerization rates of *N* -acetylalanyl- *N* '-methylamide. *Biopolymers* **1992**, *32*, 523–535.

(59) Berendsen, H. J. C.; Postma, J. P. M.; van Gunsteren, W. F.; DiNola, A.; Haak, J. R. Molecular dynamics with coupling to an external bath. *The Journal of Chemical Physics* **1984**, *81*, 3684–3690, eprint: https://pubs.aip.org/aip/jcp/article-pdf/81/8/3684/18950084/3684_1_online.pdf.

(60) Lee, T.-S.; Radak, B. K.; Pabis, A.; York, D. M. A New Maximum Likelihood Approach for Free Energy Profile Construction from Molecular Simulations. *Journal of Chemical Theory and Computation* **2013**, *9*, 153–164, PMID: 23457427.

(61) Lee, T.-S.; Radak, B. K.; Huang, M.; Wong, K.-Y.; York, D. M. Roadmaps through Free Energy Landscapes Calculated Using the Multidimensional vFEP Approach. *Journal of Chemical Theory and Computation* **2014**, *10*, 24–34, PMID: 24505217.

(62) Loibl, S.; Manby, F. R.; Schütz, M. Density fitted, local Hartree–Fock treatment of NMR chemical shifts using London atomic orbitals. *Molecular Physics* **2010**, *108*, 477–485.

(63) Loibl, S.; Schütz, M. NMR shielding tensors for density fitted local second-order Møller–Plesset perturbation theory using gauge including atomic orbitals. *The Journal of Chemical Physics* **2012**, *137*, 084107.

(64) Werner, H.-J.; Knowles, P. J.; Manby, F. R.; Black, J. A.; Doll, K.; Heßelmann, A.; Kats, D.; Köhn, A.; Korona, T.; Kreplin, D. A. et al. The Molpro quantum chemistry package. *The Journal of Chemical Physics* **2020**, *152*, 144107.

(65) Werner, H.-J.; Knowles, P. J.; Knizia, G.; Manby, F. R.; Schütz, M. Molpro: a general-purpose quantum chemistry program package. *WIREs Computational Molecular Science* **2012**, *2*, 242–253.

(66) Rusakova, I. L.; Rusakov, Y. Y. Modern Quantum Chemistry Methodology for Predicting ³¹P Nuclear Magnetic Resonance Chemical Shifts. *International Journal of Molecular Sciences* **2026**, *27*.

(67) Werner, H.-J.; Manby, F. R.; Knowles, P. J. Fast linear scaling second-order Møller-Plesset perturbation theory (MP2) using local and density fitting approximations. *The Journal of Chemical Physics* **2003**, *118*, 8149–8160.

(68) Benda, L.; Sochorová Vokáčová, Z.; Straka, M.; Sychrovský, V. Correlating the ³¹P NMR Chemical Shielding Tensor and the ²J³¹P,¹³C Spin–Spin Coupling Constants with Torsion Angles ζ and α in the Backbone of Nucleic Acids. *The Journal of Physical Chemistry B* **2012**, *116*, 3823–3833, PMID: 22380464.

(69) Marr, K. A.; Korenchan, D. E.; Jerschow, A. Influence of Magnesium Ion Binding on the Adenosine Diphosphate Structure and Dynamics, Investigated by ³¹P NMR and Molecular Dynamics Simulations. *The Journal of Physical Chemistry B* **2024**, *128*, 8966–8973, PMID: 39254719.

(70) Benda, L.; Schneider, B.; Sychrovský, V. Calculating the Response of NMR Shielding Tensor σ (³¹P) and $2J$ (³¹P,¹³C) Coupling Constants in Nucleic Acid Phosphate to Coordination of the Mg²⁺ Cation. *The Journal of Physical Chemistry A* **2011**, *115*, 2385–2395, PMID: 21366222.

(71) Buchner, R.; Hefter, G. Interactions and dynamics in electrolyte solutions by dielectric spectroscopy. *Phys. Chem. Chem. Phys.* **2009**, *11*, 8984–8999.

(72) Kundu, A.; Schauss, J.; Fingerhut, B. P.; Elsaesser, T. Change of Hydration Patterns

upon RNA Melting Probed by Excitations of Phosphate Backbone Vibrations. *The Journal of Physical Chemistry B* **2020**, *124*, 2132–2138, PMID: 32101008.

(73) Elsaesser, T.; Schauss, J.; Kundu, A.; Fingerhut, B. P. Phosphate Vibrations Probe Electric Fields in Hydrated Biomolecules: Spectroscopy, Dynamics, and Interactions. *The Journal of Physical Chemistry B* **2021**, *125*, 3899–3908, PMID: 33834783.

(74) Rao, B. D.; Buttlair, D. H.; Cohn, M. ^{31}P NMR studies of the arginine kinase reaction. Equilibrium constants and exchange rates at stoichiometric enzyme concentration. *Journal of Biological Chemistry* **1976**, *251*, 6981–6986.

(75) Granot, J.; Feigon, J.; Kearns, D. R. Interactions of DNA with divalent metal ions. I. ^{31}P -nmr studies. *Biopolymers* **1982**, *21*, 181–201.

(76) Gong, B.; Chen, J.-H.; Bevilacqua, P. C.; Golden, B. L.; Carey, P. R. Competition between $\text{Co}(\text{NH}_3)_{63+}$ and Inner Sphere Mg^{2+} Ions in the HDV Ribozyme. *Biochemistry* **2009**, *48*, 11961–11970, PMID: 19888753.

(77) Cheetham, A. K.; Clayden, N. J.; Dobson, C. M.; Jakeman, R. J. B. Correlations between ^{31}P n.m.r. chemical shifts and structural parameters in crystalline inorganic phosphates. *J. Chem. Soc., Chem. Commun.* **1986**, 195–197.